Impact of Atmospheric Rivers on Future Poleward Moisture Transport and Arctic Climate Variability

M. Kolbe[1], J. P. J. Sonnemans[3], R. Bintanja[1,2], E. C. van der Linden[2], K. van der Wiel[2], K. Whan[2], and I. Benedict[3]

[1]Faculty of Science and Engineering, Energy and Sustainability Research Institute Groningen, University of Groningen, Nijenborgh 6/7, 9747 AG Groningen, Netherlands.
[2]Royal Netherlands Meteorological Institute (KNMI), Utrechtseweg 297, 3731 GA De Bilt, Netherlands.
[3]Meteorology and Air Quality Group, Wageningen University and Research (WUR), Droevendaalsesteeg 3, 6708 PB Wageningen, Netherlands.

Key Points:

- The additional poleward moisture transport in warmer climates is almost exclusively due to atmospheric rivers.
- Higher atmospheric moisture levels are dominant in setting future atmospheric rivers increases, while dynamical changes are of secondary importance.
- Atmospheric rivers are closely related to changes in regional mid-latitude jet properties and have a strong local effect on the Arctic climate.

Corresponding author: Marlen Kolbe, `m.kolbe@rug.nl`

Abstract

Alongside mean increases in poleward moisture transport (PMT) to the Arctic, most climate models also project a linear increase in the interannual variability (IAV) with future warming. It is still uncertain to what extent atmospheric rivers (ARs) contribute to both the mean and the IAV increase of PMT. We analyzed large-ensemble climate simulations to 1) explore the link between PMT and ARs in the present-day (PD) and in two warmer climates (+2°C and +3°C compared to pre-industrial global mean temperature), 2) assess the dynamic contribution to changes in future ARs, and 3) analyze the effect of ARs on Arctic climate on interannual timescales. We find that the share of AR-related PMT (ARPMT) to PMT increases from 42% in the PD to 53% in the +3°C climate. The increase in AR-frequency and intensity is almost exclusively caused by significantly higher atmospheric moisture levels, while dynamic changes can regionally amplify or dampen the moisture-induced increase in ARs. The amount of ARs reaching the Arctic in any given region and season strongly depends on the regional jet stream position and speed southwest of this region. Our results indicate that positive ARPMT anomalies are profoundly linked to increased surface air temperature and precipitation, especially in the colder seasons, and have a predominantly negative effect on sea ice. AR events are expected to strongly affect Arctic climate variability in the future, when any AR-induced temperature anomaly occurs in an already warmer Arctic and a larger share of precipitation falls as rain.

Plain Language Summary

With ongoing global warming, the amount of moisture transported to the Arctic — and its interannual variability (or year-to-year fluctuations) — will increase. While the former can be explained by a higher water holding capacity of the atmosphere, the cause of the latter is still uncertain. In this study we link the interannual variability of poleward moisture transport (PMT) to atmospheric rivers (ARs), which are long narrow zones of relatively high water vapor content. Using a fully coupled global climate model, we detected ARs in a present-day and two warmer climates. We find that the vast majority of the future increase in PMT is caused by more frequent and intense ARs. While the increase in ARs is largely caused by higher moisture levels, our results also point to a dynamic influence. For example, a regional poleward shift and increased speed of the jet stream is associated with more ARs to the northeast. We also see significantly higher surface temperature and precipitation rates near regions of anomalously high AR activity in all seasons, and a predominantly negative response of sea ice to ARs. These linkages persist in a warmer climate, implying an increase in AR-related rainfall and the intensity of high temperature events.

1 Introduction

Multiple studies have recently linked the increased presence of atmospheric rivers (ARs) to enhanced Arctic warming, sea ice loss, and precipitation extremes (e.g. Vázquez et al., 2018; Barrett et al., 2020; Hegyi & Taylor, 2018; Komatsu et al., 2018; Nash et al., 2018). Due to their potentially severe impacts on Arctic communities and ecosystems, there is large interest in determining the processes behind years of high AR occurrences and intensity. While in some regions ARs can be of benefit (e.g. by supplying water to dry areas in the mid-latitudes), Arctic ARs are mainly associated with negative impacts: flooding of Arctic communities (Bachand & Walsh, 2022), melting of the Greenland Ice Sheet (GrIS) (Wang et al., 2020; Neff, 2018; Mattingly et al., 2018), and sea ice loss (Gimeno et al., 2015; Wang et al., 2020; Hegyi & Taylor, 2018). Still, other studies suggest they can also supply protective snow mass on land and sea ice (Mattingly et al., 2018; J. Stroeve et al., 2022; Light et al., 2022; Nghiem et al., 2016; Webster et al., 2019; P. Zhang et al., 2023).
In the absence of a strict physical definition of what exactly defines ARs, they commonly refer to low-tropospheric long narrow zones of relatively high water vapor content. Often, they are associated with cyclonic and anti-cyclonic activity and net moisture transports from lower to higher latitudes nested in large-scale circulation patterns (Zhu & Newell, 1998; Rutz et al., 2014; Z. Zhang et al., 2019; Guo et al., 2020; Woods et al., 2013). Compared to the frequent and intense AR occurence at lower latitudes, the number of ARs reaching the relatively dry and cold Arctic is small. However, a number of studies have revealed a significant increase in Arctic ARs in response to global warming, mainly owing to the expected increase in moisture alongside higher temperatures, following the Clausius-Clapeyron relation (P. Zhang et al., 2021; O'Brien et al., 2022; Allan et al., 2014; Espinoza et al., 2018).

Next to thermodynamic causes, P. Zhang et al. (2021) and Sousa et al. (2020) attribute the increase in Arctic ARs to a poleward shift of the polar jet stream related to both thermodynamic and dynamic changes. While the cause of this poleward shift is still debated, most studies attribute it to a tropical ocean warming- related shift of the sinks or sources of Rossby waves (Rivière, 2011; Chen & Held, 2007; Kidston & Gerber, 2010; Wu et al., 2011; Tandon et al., 2013). The signal of this poleward shift (linked to ocean warming) is not very strong and inconsistent across climate models, partly because Arctic sea ice loss counteracts the response by favouring an equatorward shift of the jet stream (Screen et al., 2022; Ma et al., 2021; Smith et al., 2022; Peings & Magnusdottir, 2014; Screen et al., 2013). Screen et al. (2022) suggested that the equatorward shift — caused by a sea ice loss-induced decreased meridional temperature difference in the lower troposphere — wins over the poleward shift if it is constrained by observations. In most current global climate models (GCMs) however, the sea ice signal is (too) weak, causing the poleward shift to dominate (Yim et al., 2016;

Barnes & Screen, 2015; Payne et al., 2020; Hall et al., 2015). This may partly contribute to the general increase in simulated Arctic ARs, which are very sensitive to the mean position of the storm tracks.

It is less clear how the interannual variability (IAV) of Arctic ARs (e.g. increased AR-IAV or variability of mean AR pathways) responds to the interplay of thermodynamic and dynamic changes. Overall, the response of AR variability to the combination of these regional and large-scale mean changes is poorly studied. Until now, years with increased moisture intrusions into the Arctic have been linked to anomalous pressure systems in the vicinity of AR-pathways, which favour the river-shaped intrusions and are often linked to large-scale planetary waves (Woods et al., 2013; Papritz & Dunn-Sigouin, 2020; Komatsu et al., 2018; Bao et al., 2006; H.-M. Kim & Kim, 2017; B.-M. Kim et al., 2017). For example, pronounced ridge–trough patterns during negative phases of the North Atlantic Oscillation (NAO) allow ARs to reach western Greenland (C. Liu & Barnes, 2015; Neff, 2018), while positive phases of the NAO have been associated with increased ARs over northern and western Norway (I. Benedict et al., 2019). These studies suggest that teleconnection patterns can greatly influence ARs in distinct Arctic regions. It is likely that more large-scale patterns such as the Arctic Oscillation may have an Arctic-wide impact, but so far there is no clear evidence for a significant Arctic-wide increase in ARs associated with any large-scale mode of climate variability.

Based on the Coupled Model Intercomparison Project (CMIP) 6 projections, Ma & Chen (2022) have further concluded that winter ARs over the Northern Pacific are strongly influenced by tropical sea surface temperature forcing, while ARs over the Northern Atlantic mainly depend on the internal variability of the atmosphere. The drivers and effects of AR variability in most studies have mainly been identified using observation-based or short-term present-day model data. To our knowledge, so far no study has evaluated Arctic ARs using long continuous coupled model simulations, which allows for a more robust discussion of AR-IAV including its drivers and impacts. Studies on future Arctic AR activity based on GCMs mainly address changes in the mean state of AR characteristics instead of drivers of IAV, focus on a particular season, or do not cover the entire Arctic region (Gao et al., 2015; Shields & Kiehl, 2016; Warner et al., 2015; Warner & Mass, 2017; Payne et al., 2020).
Non-AR related Arctic studies discussing future climates point towards a considerable increase in the IAV and number of extreme rainfall and melt events over the Arctic (Bogerd et al., 2020; van der Wiel & Bintanja, 2021; C. Liu & Barnes, 2015), which could be severely affected by fluctuations of annual AR occurrences. The simulated increase in Arctic precipitation IAV has previously been linked to the respective increase in the IAV of poleward moisture transport (PMT) (Bintanja et al., 2020; Bogerd et al., 2020; Skific et al., 2009a,b).

While the increase in mean PMT was found to mainly occur due to enhanced atmospheric moisture levels following atmospheric warming, the precise causes of the IAV increase are still uncertain (Bintanja et al., 2020; X. Zhang et al., 2013; Bogerd et al., 2020). Similar to the lack of knowledge concerning future AR-IAV, one of the main reasons for this is that PMT-IAV is largely effected by dynamic changes of the atmosphere and therefore sensitive to changes of the location of the jet stream and characteristics of storms reaching the Arctic. There is no established consensus around the future of planetary-scale climate modes and the synoptic scale circulation, which by default are chaotic in nature and sensitive to climatic changes (Hall et al., 2015; Payne et al., 2020; Tan et al., 2020). The combined increase of mean and IAV of PMT translates into an increased intensity of extreme events in the Arctic (Bintanja & Selten, 2014; Pendergrass et al., 2017; van der Wiel & Bintanja, 2021), making it crucial to consider changes in variability.

This study examines both mean and IAV changes of the intensity and frequency of Arctic ARs. Variability is generally best identified over relatively long time periods or stable climate conditions without strong changes in mean trends. In order to robustly define IAV changes from the present-day to future climates, we therefore assess ARs in large-ensemble 5-year runs branched from three different periods of the EC-Earth2.3 RCP8.5 scenario. These three climate runs represent the present-day climate (hereafter PD), as well as a +2°C and a +3°C warmer than PI climate as further described in section 2.1. By calculating ARs for the future climates in two different ways (see section 2.2), we aim to separate the thermodynamic (moisture-induced) from the dynamic (circulation-induced) effect. With this distinction we are able to assess whether changes in AR(-IAV) are dominantly caused by shifts in wind patterns or by increased integrated water vapour levels. As we foresee both regional and seasonal non-homogeneity in the change of ARs and their driving mechanisms, we further distinguish between different seasons, and define the AR responses for four different Arctic sectors, as described in section 2.2.

The first part of this work (section 3.1) discusses future changes in the relation between ARs and PMT, while the second part (section 3.2) addresses the dynamical influence as well as seasonal and regional differences in these AR(-IAV) changes. Finally, section 3.3 focuses on the direct effects of ARs on Arctic surface air temperature (SAT), precipitation (PR), and sea ice concentration (SIC).

2 Methodology

2.1 Data

We use three different EC-Earth2.3 large ensembles to investigate AR dynamics in present and future climates. Three initial-condition large ensembles were branched off from a

16-member historical+RCP8.5 experiment. A more detailed explanation of the construction of the large ensembles is given in van der Wiel et al. (2019).

EC-Earth is a GCM based on the atmospheric integrated forecast system (IFS) of ECMWF, coupled to an ocean model (Nucleus for European Modelling of the Ocean, NEMO) with modules for sea ice (Louvain-la-Neuve, LIM2) and land components (Tiled ECMWF Surface Exchanges over Land incorporating land surface hydrology, HTESSEL) (Hazeleger et al., 2012). To contend with a cold bias over the Arctic region (Koenigk et al., 2013), the present-day ensemble uses the model period 2035-2039 (experiment referred to as PD). The simulated global mean surface temperature (GMST) of this period best matches the observed GMST from 2011 to 2014. The two future climate scenarios are based on a GMST increase of 2°C relative to PI (2062-2066 equivalent) and a GMST increase of 3°C relative to PI (2082-2086 equivalent). Each climate simulation consist of 2,000 simulated years of global, daily data at 1.125° x 1.125° resolution for the atmosphere (van der Wiel et al., 2019). For the seasonal analysis, we had to omit one year of each 5-year run (the first year for DJF, and the fifth year for remaining seasons), resulting in 1,600 years for each season and climate.

To detect ARs and calculate PMT, we obtained the daily specific humidity and the wind speed in zonal and meridional directions at four pressure levels (1000, 850, 500, 200 hPa) from each climate ensemble. In addition, SAT, PR and SIC are analyzed to assess the impact of ARs on Arctic climate indicators.

To validate the model data for the PD climate, we used monthly ERA5 reanalysis fields from 2005 to 2020 (Hersbach et al., 2020) and compared all variables in use here. As ERA5 has a higher spatial resolution of 0.25°, we regridded the field to the EC-Earth grid. Validation results are discussed in section 2.5.

2.2 Detection of Arctic ARs

The first AR detection criteria a northward directed meridional IVT-component and a minimum length/width ratio of 2 (Guan & Waliser, 2015). We defined the length as the maximum extension of an AR object, while the width is defined by the object surface area divided by the length. To be classified as an Arctic AR, the AR-pathway should cross 70°N.

Generally following the detection algorithm from Rutz et al. (2014), we calculated ARs based on ERA5 and the three different EC-Earth climates. For each grid point, we first calculated the integrated water vapour transport (IVT) as:

$$IVT = \frac{1}{g} \int_{p_0}^{p_1} q\mathbf{V} dp, \tag{1}$$

where g is the gravitational acceleration (m s^{-2}), q is the specific humidity (kg kg^{-1}), $\mathbf{V}$ is the horizontal wind vector (m s^{-1}), consisting of a u and v component, and p_0 (p_1) is the surface pressure (upper boundary) level in hPa. We integrated from 200 hPa to 1000 hPa, using the 1000 hPa, 850 hPa, 500 hPa and 200 hPa pressure levels. Based on a sensitivity analysis with ERA5, we did not find significant differences when calculating IVT using 50 levels from 1000-300 hPa instead of the 4 levels in this study, from which we assume sufficient accuracy of our IVT-calculation.

We define local IVT thresholds based on the IVT climatology to compute ARs. While most of the detection algorithms covered in latest reports of the Atmospheric River Tracking Method Intercomparison Project (ARTMIP) agree on a minimum AR length threshold of 2,000 kilometers (Rutz et al., 2019; Collow et al., 2022), there is higher disparity in the IVT-thresholds across global AR studies. This inconsistency should not be avoided according to Shields et al. (2018) and Rutz et al. (2019), as every study addresses a specific question. However, the ARTMIP community suggests to include a sensitivity analysis by conducting AR calculations with slight adjustments to the algorithm. In addition to the commonly used grid-point-based IVT>85^{th} percentile threshold, we therefore decided to apply three varying minimum thresholds of 50, 70 and 90 kg m^{-1} s^{-1} to detect Arctic ARs. These minimum thresholds only take effect when the local 85^{th} percentile is met, which is illustrated for the present-day in Figure 1 a-c. Based on our research objective and in order to be consistent with Nash et al. (2018) and Guan & Waliser (2015), we focus our analysis using the lowest minimum IVT threshold for the present-day ARs, i.e. 50 kg m^{-1} s^{-1}. This choice allowed us to include present-day ARs with slightly lower moisture transport but potentially strong effects on the usually dry Arctic climate. Figure 1 a-c shows the effect of the different thresholds, where the mean IVT of the PD climate is plotted behind a mask of the respective minimum thresholds. This illustrates the regions where the minimum thresholds come into effect in the PD runs. The lower panel (d-f) illustrates an example of a winter AR only detected with the 50 kg m^{-1} s^{-1} minimum threshold, highlighting the cold and dry Greenland Ice Sheet (GrIS) as one of the main regions affected by the choice of threshold. On this particular day, the IVT value of the AR over the GrIS is between 50 and 70 kg m^{-1} s^{-1}. Featured is also the tip of a detected AR over East Siberia excluded from our study as it does not cross 70°N.

For detecting ARs in the future climates, we used two different techniques:

1) To study the absolute changes in ARs, we preserved the PD thresholds to detect ARs in a +2°C and +3°C warmer than PI climate (referred to as 2C and 3C hereafter). According to the classification provided by O'Brien et al. (2022), this choice of threshold falls

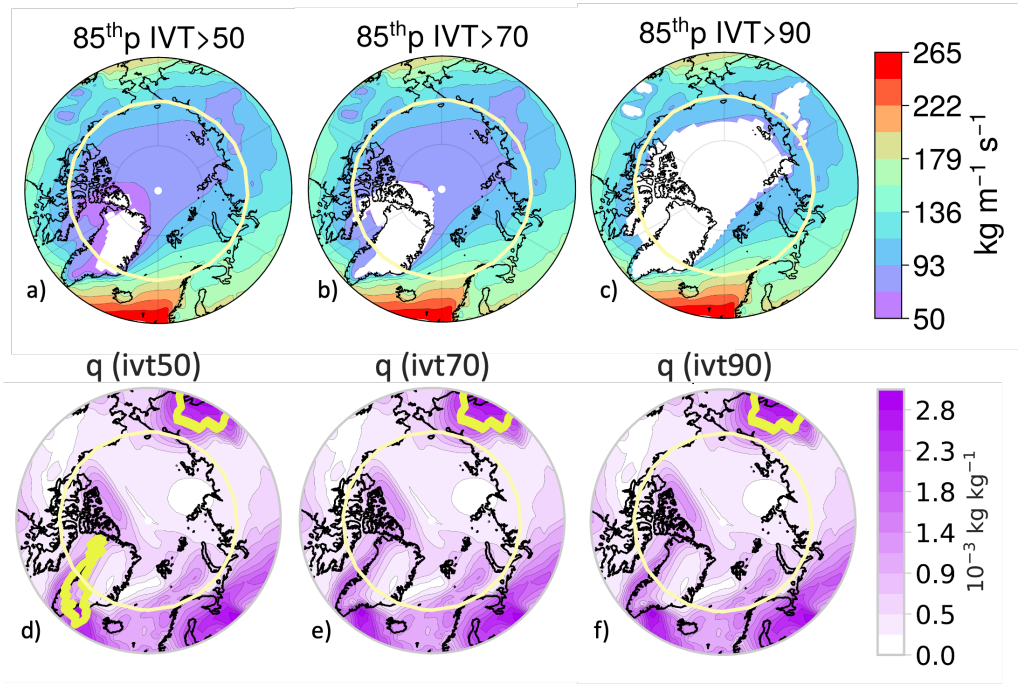

Figure 1: a-c: Present-day IVT>85th percentile in the EC-Earth runs, plotted behind three different masks indicating the effect of the minimum IVT thresholds. d-f: Specific humidity from a random EC-Earth member (in January) including an Arctic AR detected only with the lowest threshold (yellow outline over Greenland).

under the category of 'fixed relative' methods, implying that the IVT value to be exceeded is relative to the location, but fixed in time.

2) To study dynamic-sensitive AR changes unrelated to increased moisture levels, we recalculated potential future ARs using a 'relative' method (referred to as r2C and r3C hereafter). Here we calculated and used the climate-specific local IVT thresholds while retaining the minimum thresholds as described above. Due to increased moisture levels in the warmer climates, the resulting 85th percentile thresholds are thus higher, meaning that detected ARs in the r2C and r3C runs are more sensitive to dynamic changes. As almost all local 85th percentiles in the future climates exceed 50 kg m^{-1} s^{-1} (not shown), we base our analysis on dynamic-sensitive future ARs detected with the 70 kg m^{-1} s^{-1} minimum threshold, where the regions affected by the minimum threshold are very similar (Figure A1). This allows for a fair comparison of differences in the dynamic changes of ARs (we found that if we used the 50 kg m^{-1} s^{-1} minimum threshold, there was an exceptional AR increase over the region in Greenland, as the minimum threshold criteria only had to be met in the PD climate).

2.3 Quantification of (AR-related) PMT and AR-frequency

To clearly distinguish poleward moisture transport (PMT) from equatorward moisture transport (EMT) along 70°N, we used the PMT calculation from Bengtsson et al. (2011):

$$PMT = \frac{1}{g} \oint_L \int_{p_0}^{p_1} q\mathbf{V_n} dp dl, \tag{2}$$

where g is the gravitational acceleration (in m s^{-2}), L represents the 70°N latitude band, p_0 (p_1) is the surface pressure (upper boundary) level, q is the specific humidity (kg kg^{-1}), $\mathbf{V_n}$ the meridional wind across latitude L (in m s^{-1}), and l the latitude (between 70°N and 90°N). In addition to quantifying PMT (only poleward), EMT (only equatorward, i.e. negative PMT), and AR-related PMT (PMT across the part of the 70°N latitude band within AR-shapes), this method also allowed us to determine respective differences across longitudes along 70°N. AR-intensity is then defined as the amount of PMT within ARs at the 70°N latitude band.

We define AR-frequency as the amount of AR-shapes reaching 70°N on any given day (e.g. 2 ARs in Figure 2). ARs that last two days are therefore counted twice (if they still meet all AR detection criteria).

2.4 Division of the Arctic Region into Sectors

As shown in previous work on Arctic moisture transport, ARs typically follow favourable pathways such as the Atlantic or Pacific ocean basins (e.g. Vázquez et al., 2018; Nash et al., 2018). Here, a substantial number of ARs also reach the 70°N latitude band from continental areas in addition to the common ocean pathways. Because the main drivers of ARs in different regions may evolve differently towards a warmer climate, we present AR-IAV changes on a sector basis. We divide the Arctic into four sectors separated by four meridians (45E, 45W, 135E, 135W) as shown in Figure 2, exemplifying 2 ARs reaching the Arctic in late May, one in the Canadian sector and one in the Atlantic sector. Although the Canadian AR also reaches the Pacific sector, we only assign one sector to each AR (the one with the most amount of AR area north of 70°N). The 2 ARs in the other sectors have been detected based on their IVT and shape, but are not counted as Arctic ARs, as they do not cross 70°N (i.e. they are excluded from our statistics but serve as visual demonstrations of AR origins).

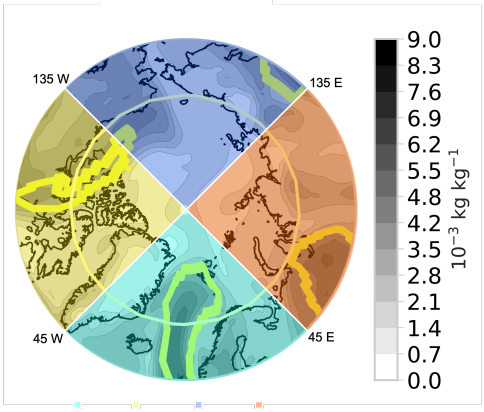

Figure 2: Illustration of the division of the Arctic region into the Atlantic (cyan), the Eurasian (orange), the Pacific (darkblue) and the Canadian (yellow) sector. Pictured is an example of 2 atmospheric rivers (ARs) reaching the Arctic region in present-day EC-Earth, superimposed on the moisture field at 850 hPa. The other ARs in the Eurasian and Pacific sector are not included in this study (only to visually demonstrate origins of ARs) as they do not not pass 70°N.

2.5 Validating ARs in EC-Earth with ERA5

Generally, there is good agreement between the frequency and intensity of ARs in EC-Earth and ERA5 (Figure 3d). ARs in ERA5 detected during 2005-2020 carry slightly more moisture (9.79 kg kg^{-1}) than those detected in the EC-Earth ensembles (9.63 kg kg^{-1}), while EC-Earth tends to detect more ARs on an annual basis (371 ARs in EC-Earth versus 346 ARs in ERA5). Still, both are of similar magnitude given the common large variance of AR characteristics (O'Brien et al., 2022). As shown in Figure 3c, EC-Earth detects slightly less ARs over the GrIS, the West Atlantic, the Kara Sea and the Pacific Central Arctic than ERA5, while more ARs are detected over the North Atlantic and lower latitudes of most continental areas north of 70°N. Although this study only assesses ARs passing 70°N, we include the latitudes between 60°N and 70°N to visualize the pathway of Arctic ARs (the spatial mean still only refers to the area north of 70°N). When comparing AR-days of all grid points, EC-Earth detects 0.45 more AR-days per year than ERA5. In terms of spatial patterns and magnitude, these results are nearly identical across the three different minimum IVT thresholds (not shown).

Additionally, we compared the variables that impact or are associated with ARs (see section 3.3: Impacts of ARs on Arctic climate). Figure A2 shows the difference between EC-Earths and ERA5s average SAT, PR and SIC. In brief, the difference in the temporal mean is small for all variables, while EC-Earth is cooler over Greenland and the Central Arctic Ocean and Pacific sector, but warmer over the the majority of the Atlantic and Eurasian

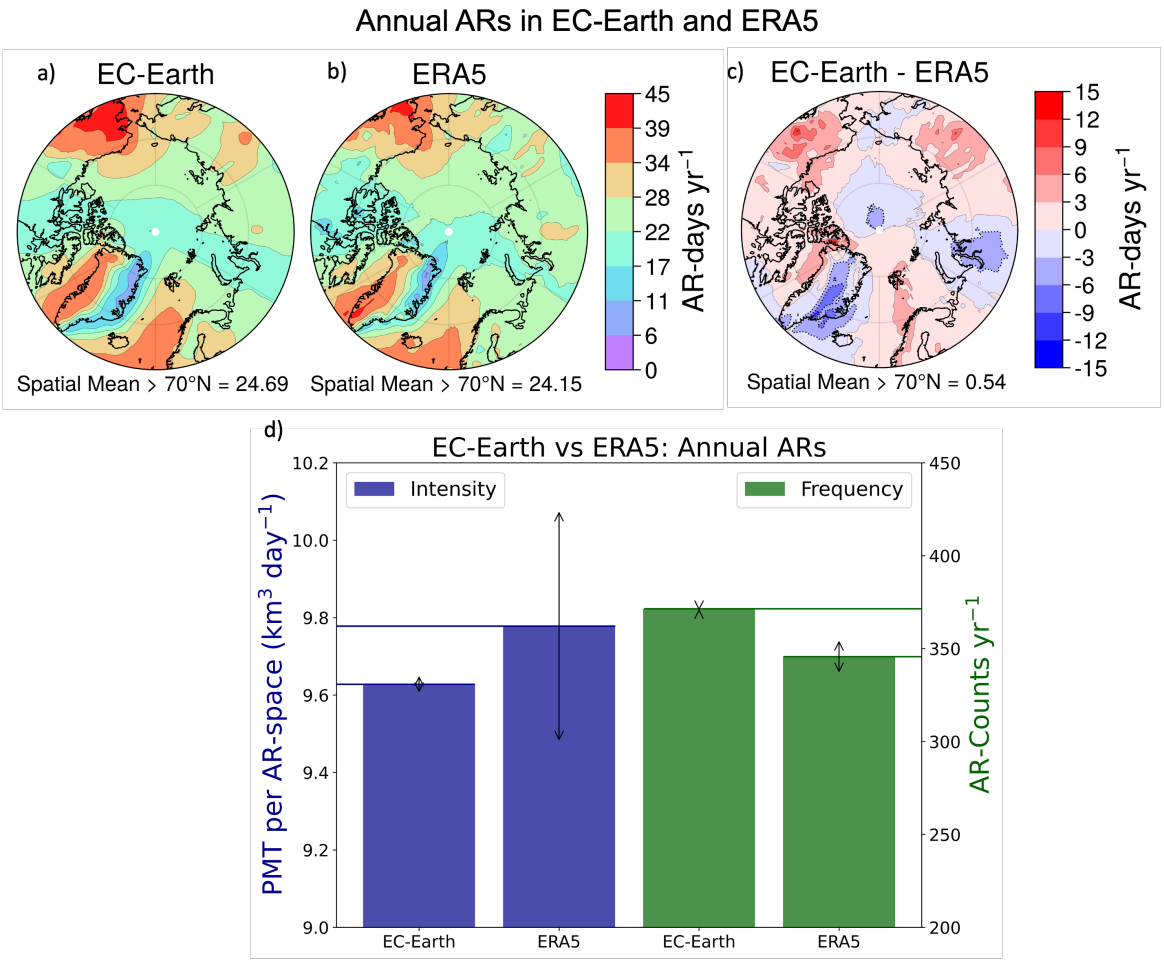

Figure 3: Annual mean AR-days in EC-Earth (a) and ERA5 (b). c: Spatial mean difference of annual AR-days: EC-Earth - ERA5 (red = more AR-days in EC-Earth). d: Mean intensity (poleward moisture transport per AR) and frequency (counted ARs per year, including duplicates for multi-day ARs) in EC-Earth (present-day run) and ERA5 (2005-2020). Vertical grey lines represent the 95^{th} confidence intervals (for EC-Earth frequency only [370.5,372.4]).

sector. Correspondingly, the slightly warmer (cooler) regions in EC-Earth exhibit higher (lower) PR and lower (higher) SIC.

3 Results and Discussion

For the majority of the study we analyse future ARs detected using the 'fixed relative' method (2C and 3C ARs) in order to focus on the absolute changes that occur from the PD to warmer climates. In section 3.2 we further investigate future ARs detected using the 'relative' method (r2C and r3C ARs) to study the contribution of dynamic changes to future ARs.

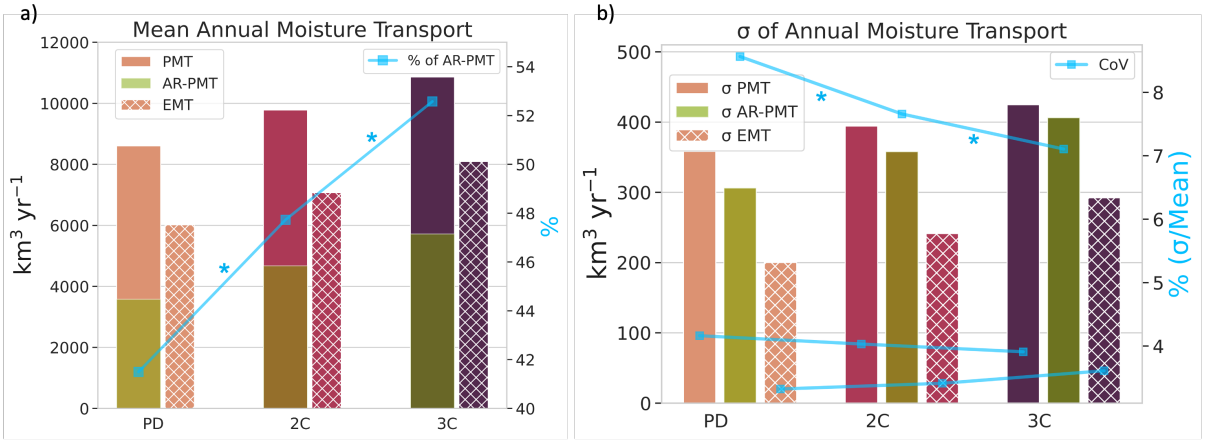

Figure 4: a: Annually averaged poleward moisture transport (PMT), AR-related PMT (ARPMT), and equatorward moisture transport (EMT) in the present-day (PD), +2°C warmer than PI (2C), and +3°C warmer than PI (3C) climates. The increase of AR-related PMT to total PMT is illustrated by the blue line, with the percentage of ARPMT displayed on the right y-axis. b: Interannual variability (IAV) of PMT, ARPMT, and EMT in the three climates. The respective increases in IAV relative to the mean increase (Coefficient of Variation, CoV) are illustrated by the blue lines, with the percentage displayed on the right y-axis. The stars next to the CoV lines indicate that the change from climate to climate is significant (p-value of ttest < 0.05).

3.1 Changes in (AR-related) Poleward Moisture Transport

In order to discuss climate-related AR-changes in the context of increased PMT, we first identify the spatial mean changes of moisture transport across 70°N. We note an increase in annual mean PMT towards warmer climates (Figure 4a), consistent with previous studies (Bintanja et al., 2020; Bogerd et al., 2020; P. Zhang et al., 2021). Furthermore, the relative percentage of ARPMT to total PMT increases by 11%, which is roughly consistent across all four seasons (Figure 5a,c,d,g). The relative percentage of ARPMT is much higher in the warmer months (in all three climates), which is partly a side effect of our choice of an annually uniform IVT threshold. Nash et al. (2018) used seasonal-specific thresholds and still found that the share of Arctic ARPMT to total PMT is largest in summer. The increase in ARPMT/PMT ratio alongside an increase in mean PMT appears in all seasons, and indicates that the extra PMT is mainly caused by more frequent and/or more intense ARs. Annually averaged, 95% of the additional PMT from the PD to the 3C climate is transported through ARs (ΔARPMT /ΔPMT = 0.948). Obviously, this number is very sensitive to the AR definition: here we refer to ARPMT in the 3C experiment, and thus all relatively concentrated PMT plumes can easily exceed the IVT>85$^{\text{th}}$ percentile threshold of the PD climate and be counted as an AR.

Although PMT-IAV also linearly increases from the PD to the 3C climate (Figure 4b), the variability increase is moderate compared to that of the mean. This is demonstrated by

a small (and insignificant) decrease in the Coefficient of Variation (CoV; standard deviation divided by the mean) of PMT from PD to warmer climates (blue lines in Figure 4b). While the negative CoV trend of PMT is small and mainly insignificant in our simulations and in CMIP6 data, it is present in all seasons, and even significant in spring (from PD to 2C; Figure 5b). Using the simplified PMT method (area-averaged precipitation minus evaporation) in contrast suggests a small disproportional increase in PMT-IAV relative to its mean (i.e. slightly increased CoV). A small disproportional increase of variability is also apparent in the CMIP5 (Bintanja et al., 2020) and CMIP6 simulations (tested based on 31 CMIP6 models, where the change in PMT-CoV was also not significant). One reason for the inconsistency in the sign of the CoV across different methods may be that the simplified PMT calculation assesses the net moisture to and from the Arctic, which thus does not distinguish poleward from equatorward moisture transport (EMT). This idea is supported by the slight increase in EMT (Figure 4b) in our simulations (which however is not significant at least on an annually averaged basis), and highlights the importance of strictly differentiating between the northward and southward component of moisture transport.

Our results thus suggest that the increase in (strictly northward) PMT-IAV is fairly weak and mainly a secondary effect of increased mean PMT. The CoV of AR-related PMT also decreases significantly, both annually (Figure 4b) and in all seasons (Figure 5b,d,f,h), implying a more consistent, relatively less variable AR-associated moisture transport to the Arctic in warmer climates. This CoV decrease of ARPMT can thus explain the CoV decrease in total PMT, taking into account the high ARPMT-to-PMT share in warmer climates (Figure 4a).

To summarize, Arctic ARs transport nearly all additional poleward moisture in future climates, and their contribution to Arctic moisture transport becomes more consistent and relatively less variable. We found that ARPMT is slightly lower using the two higher thresholds (Figure A3), but the results were not qualitatively effected by this. So far, the AR changes towards the warmer climates are based on the simulations where the same moisture threshold as that for the PD detection is used. We will now also assess the climate-relative AR simulations (r2C and r3C) to investigate if the changes are at least partly dynamically-driven. Additionally, we address whether the increase in AR-related PMT is caused by increased frequency or intensity of ARs.

3.2 Dynamic and Thermodynamic Changes of ARs and AR-IAV across Seasons and Sectors

Based on the results above, this section addresses the following questions:

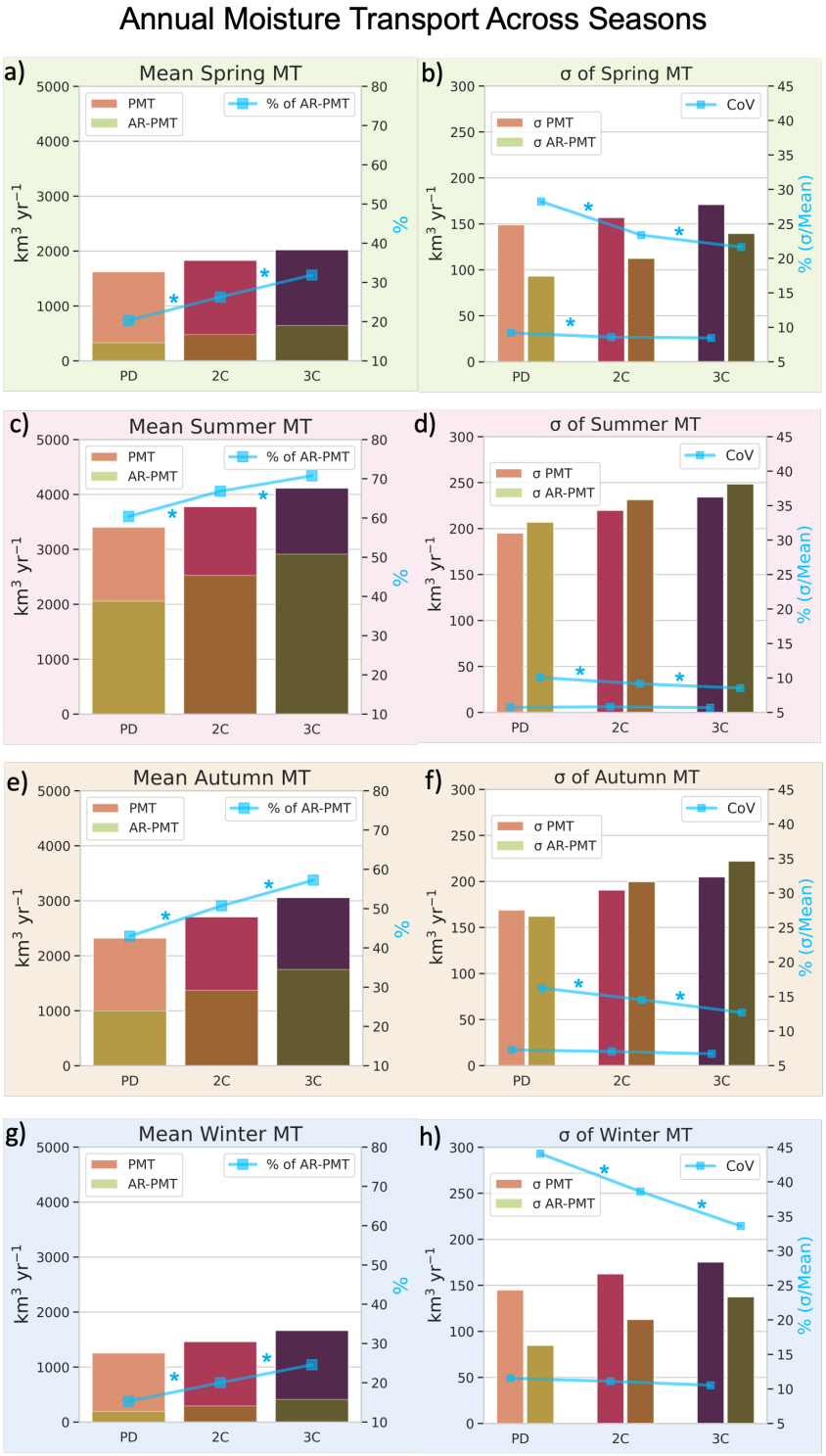

Figure 5: As in Figure 4, but on a seasonal basis and without equatorward moisture transport (EMT). a&b: Spring (MAM). c&d: Summer (JJA). d&f: Autumn (SON). g&h: Winter (DJF).

1) *Where and when do ARs and AR variability increase most, and are these changes partly circulation-driven or due to higher moisture levels?*

2) *What increases more: the frequency or the intensity of ARs and AR variability?*

3) *Does the jet position (latitude) drive the interannual variability of Arctic ARs?*

To address these questions simultaneously, we present regional and seasonal changes while introducing changes in the characteristics of ARs detected using climate-relative IVT thresholds (ARs in the r2C and r3C simulations).

3.2.1 Where and when do ARs and AR variability increase most, and are these changes partly circulation-driven?

Here we discuss dynamic and thermodynamic changes in the occurrence of ARs and their variability. The strongest increase in AR-days from the PD to the 3C climate occurs over the North Atlantic storm track region, the western GrIS and Northwestern Canada (Figure 6b), where ARs are already most frequent (Figure 6a). North of 70°N, the occurrence of AR-days increases by 15 days per year (mainly in summer and autumn; Figure A4c&e), with up to 26 additional days over the North Atlantic. Most ARs reaching the deeper Arctic in warmer climates originate from the Atlantic sector (across the Norwegian Sea), which is in line with current trends (Vázquez et al., 2018), and applies to all seasons (Figure A4). These ARs are of particular importance, as, from a relative perspective, AR-days increase most over the Central Arctic Ocean (Figure 6c). In particular, ARs over the Northeast GrIS, as well as regions north of the Fram Strait and the Barents Sea occur more than twice as often in the 3C compared to the PD climate. This could imply a dynamical (northward) shift of ARs, but the Central Arctic is also the region where the relative increase in specific humidity is strongest (Figure 7c), which increases the likelihood of fulfilling the detection criteria.

In fact, we do not find a substantial increase in annual mean Arctic AR-days if we adjust the IVT threshold (r3C experiment; Figure 6d), which further implies that the absolute increase is mainly moisture-driven. Rather, the dynamic response is mostly negative (fewer AR-days), especially over the GrIS. In r3C, there are up to 6 fewer AR-days over the GrIS and 2-3 fewer AR-days over the majority of the Arctic Ocean, except for the Atlantic sector. The wind components and the sea level pressure (SLP) change from the PD to the 3C climate indicate an strengthening of the Greenland Blocking High (GBH): while SLP decreases over the entire Arctic Ocean, it increases over the Central GrIS (Figure 7d), corresponding to a strengthening (weakening) of meridional winds east (west) of Greenland (Figure 7g). Although the regional patterns and changes in magnitude may be model-dependent, these

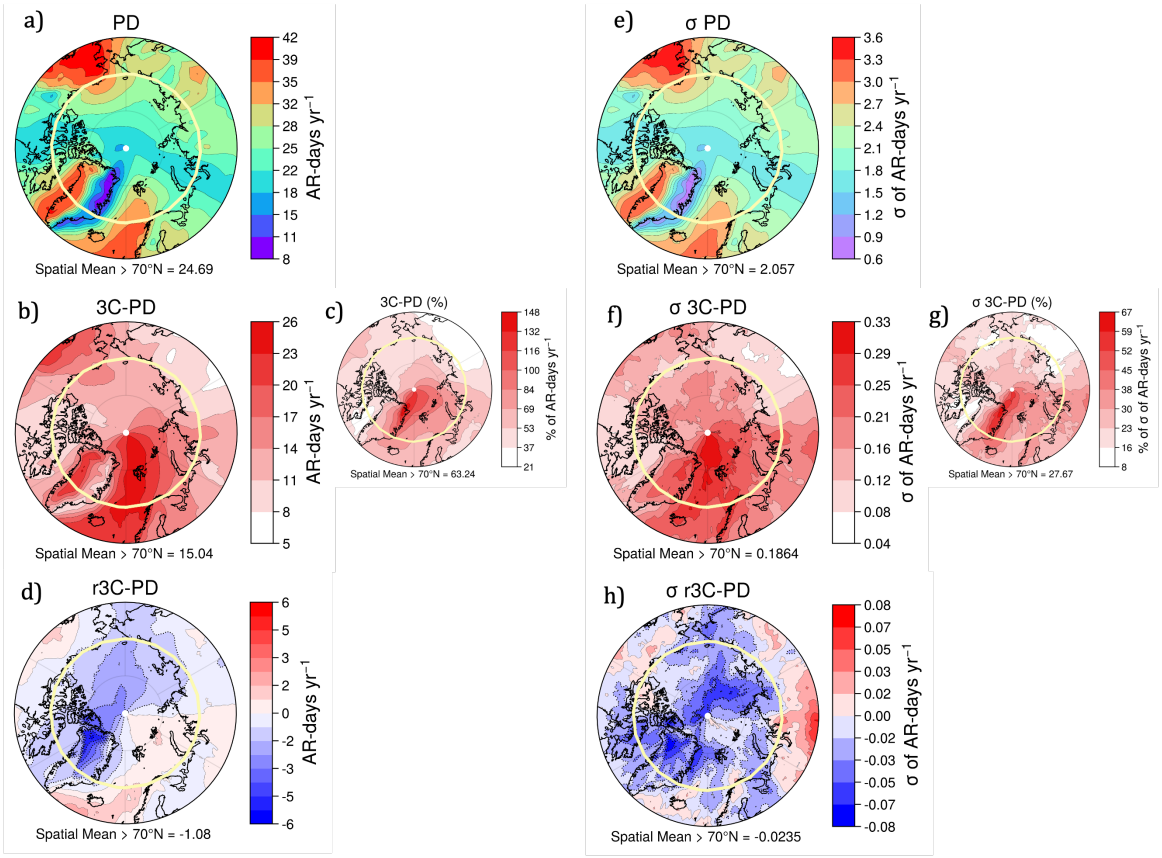

Figure 6: Left panel: Present-day annual AR-days per grid point (a), and their absolute increase towards the 3C climate (b). Side plot c shows this increase relative to the location. d: Same as b) but based on the r3C runs, thus representing differences in AR-days caused by mainly dynamic changes. Right panel (e-h): Same as left panel except for interannual variability (standard deviation of annual means).

trends have already been identified using observation-based data, and linked to enhanced summer and winter moisture transport to the GrIS (Barrett et al., 2020; Rimbu et al., 2007). In EC-Earth, the increase in Greenland blocking only occurs during winter and spring (Figure A4i,l), while in summer we see a decrease (Figure A4j,k). As the majority of our ARs occur during summer (due to the annual mean IVT threshold), this can explain why the dynamic-induced annually averaged contribution to future ARs over Greenland is negative (Figure 6d). The annual mean zonal wind response in the warmer EC-Earth climate indicates an intensification of the North Atlantic storm tracks (in line with most GCMs as mentioned above), and decreased westerlies on the Pacific side (Figure 7i). The strength of meridional winds in the eastern part of the Pacific increases, but decreases in the western and the northern part of the Pacific Arctic Ocean sector (Figure 7g). These circulation changes towards warmer climates partly drive the dynamic-sensitive AR response (Figure 6d): fewer AR-days in the Pacific sector of the Arctic Ocean, and a weak increase (up to 2 more AR-days) over the Barents and Kara seas in the North Atlantic vicinity. However,

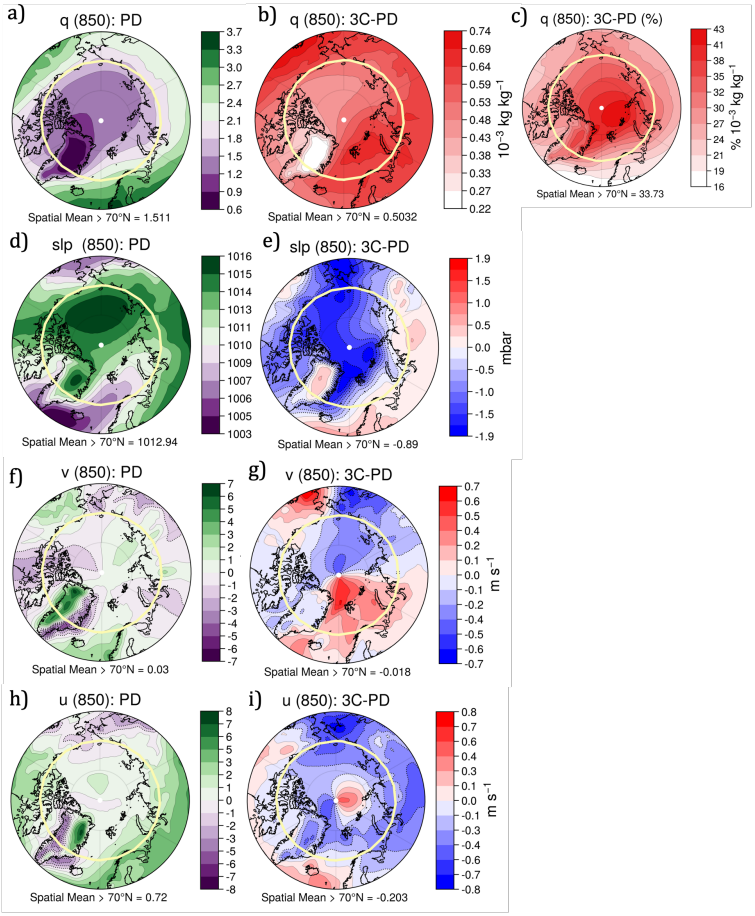

Figure 7: Present-day annual mean fields at 850 hPA of a: moisture (q); d: sea level pressure (slp); f: meridional winds (v); and h: zonal winds (u), and the difference towards the 3C climate (b,e,g,i respectively). For the moisture field, the relative increase is shown in c.

this trend is dominated by the summer season, while we see fewer (more) AR-days in the Atlantic (Pacific) sector towards the winter months (Figure A4). In section 3.2.3 we analyze the relationship of ARs and atmospheric patterns on interannual time scales on a seasonal basis.

The spatial pattern of IAV of present-day Arctic AR-days is closely related to the mean distribution, i.e. regions with higher AR occurrences also show larger year-to-year fluctuations (Figure 6e). Likewise, the IAV of AR-days increases most over the Atlantic sector of the Central Arctic Ocean (Figure 6f). Although the increase in mean AR-days is stronger over the West than over the East of Greenland, the variability increases most over the Northeast (Figure 6b; again only in summer and autumn, reversed in winter and spring - not shown). Especially from a local-% perspective, the IAV of ARs reaching the Northeast GrIS increases significantly (Figure 6g). That said, the local-% increase in IAV

is small across the entire Arctic (28% on average) compared to the local-% mean increase (63% on average) (Figure 6c). This aligns with the decrease in the CoV of ARPMT towards warmer climates (Figure 4b).

The reduced AR-day variability in response to global warming is partly caused by dynamic changes: in r3C, the IAV of AR-days is lower than at present in almost all Arctic regions (Figure 6h; but the difference is very small). It decreases most over Greenland and the Pacific sector of the Arctic Ocean (following the r3C mean - Figure 6d), however also over the Atlantic sector. While mean changes in the Arctic climate (for example increased PR and SAT) are mainly caused by local processes such as evaporation in response to sea ice loss, the IAV of Arctic climate variables is more sensitive to changes in atmospheric dynamics and lower latitudes (Bintanja et al., 2020; Higgins & Cassano, 2009; Bogerd et al., 2020; Gimeno-Sotelo et al., 2019).

To conclude, our simulations project an increase in absolute AR-days over the entire Arctic in a warmer climate. Even over regions such as the GrIS, where we see a reduction in wind transport associated with increased blocking, the increase in moisture levels result in increased AR-days, with severe potential impacts on surface melting (Mattingly et al., 2018; Neff, 2018). While we highlight strong seasonal differences, the dynamic response of AR occurrence to global warming partly explains why the majority of future ARs reach the Arctic from the Atlantic instead of the Pacific sector. As such, our results are linked with the assumption of a poleward shift of the North Atlantic storm tracks (Yim et al., 2016; Barnes & Screen, 2015; Payne et al., 2020; Hall et al., 2015, e.g.). Although the IAV of AR-days increases across the entire Arctic, we find that this increase is weak compared to that of the mean. This result aligns with the decreased CoV of ARPMT, and is likely a sign of the different processes governing mean versus IAV changes.

3.2.2 What increases more: The frequency or the intensity of ARs and AR variability?

In this part we discuss future changes in the frequency and intensity of Arctic ARs. Although AR-intensity and AR-frequency are partly linked (higher moisture levels allow for more detected ARs), this analysis provides additional insights on the potential impact per AR. The results above already indicate an increase in AR-days, while higher humidity levels (Figure 7b) further suggest that most future ARs will also carry more moisture. As the IAV increase of AR-days is relatively weak compared to the mean increase (Figure 6), this section will reveal whether this is due to a decreased CoV of AR-frequency or AR-intensity (explained in section 2.3), or both.

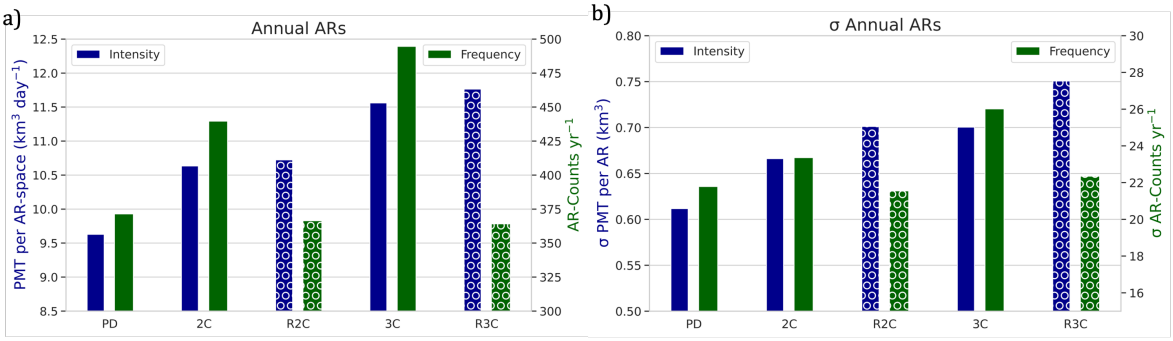

Figure 8: a: Annually averaged intensity (PMT per AR, blue) and frequency (counted ARs, green) in a present-day (PD), +2°C warmer than PI (2C), and +3°C warmer than PI (3C) climate. Bars with white circles represent the respective indices for the relative (r2C and r3C) climate ensembles. b: Same as a) but for interannual variability (IAV), defined as the standard deviation of annual means.

Figure 8a illustrates how both the intensity and frequency of Arctic ARs increase almost linearly from the PD over the 2C to the 3C climate. The intensity of ARs in the r2C and r3C simulations is not significantly higher than in the 2C and 3C climates, and the frequency of r2C and r3C ARs is even (negligibly) lower (366 and 364 ARs yr^{-1}) compared to the PD level (371 ARs yr^{-1}). In agreement with the previous findings, these results suggest that both the increased intensity and frequency in warmer climates are mostly a response to higher moisture levels instead of dynamic changes.

The dynamic influence on increased IAV of AR-frequency is likewise minor (Figure 8b). However, we do note a significantly stronger increase in the IAV of AR-intensity in r2C and r3C compared to 2C and 3C, which suggests that the annually averaged transported moisture per AR in warmer climates strongly depends on atmospheric dynamics. A reason for this may be that in 2C and 3C, variations of AR-intensity are lower because there are more (including weaker) ARs detected. Furthermore, these spatially averaged changes in intensity and frequency could be subject to compensations between different Arctic sectors.

The increases in intensity and frequency of ARs are of similar magnitude in all Arctic sectors (Figure 9a&b). To investigate frequency and intensity changes on regional scales, we focus on the four Arctic sectors (Figure 2). By scaling the changes in IAV by the mean changes of each sector (i.e. CoV), we examine whether increased fluctuations in AR activity are only a result of increases in the mean. For these analyses, we only focus on the 2C and 3C ARs, as the r2C and r3C simulations indicate similar results in terms of the CoV patterns. In the PD climate, ARs from the Pacific sector are most intense, while ARs from the Atlantic sector are significantly more frequent. The relatively low intensity over the Atlantic and Canadian sectors is likely due to the low humidity in the vicinity of the cold GrIS. However, the intensity of Atlantic sector ARs significantly increases towards the

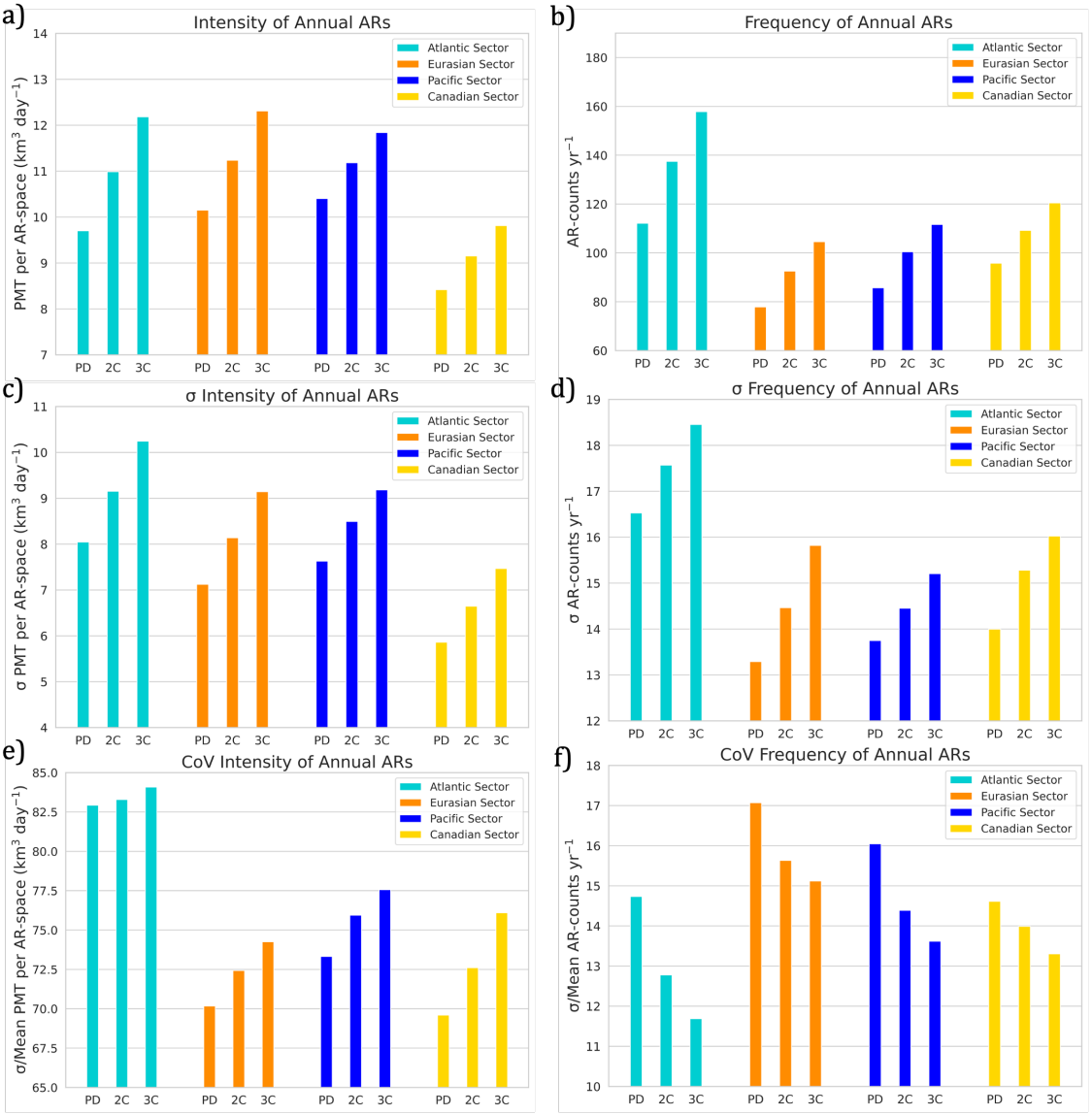

Figure 9: a: Annually averaged intensity (PMT per AR, a) and frequency (counted ARs, b) in the PD, 2C and 3C climates c&d: Same as a&b but for interannual variability (IAV, defined as the standard deviation of annual means). e&f: IAV as in c&d scaled by the mean changes in a&b.

3C climate, reaching similar levels as those of Pacific sector ARs (Figure 9a). Despite the relatively low mean intensity of Atlantic sector ARs, the annually averaged amount of PMT per AR fluctuates most over the Atlantic sector (Figure 9c). This may be caused by years with many ARs over Greenland (lower mean intensity), alternating with years with few ARs over Greenland (higher mean intensity). Otherwise, the IAV of AR-intensity and frequency roughly corresponds to the respective mean states in each sector and likewise increases over all sectors (Figure 9c&d). The CoV changes emphasize the anomalously high IAV of AR-intensity over the Atlantic sector (Figure 9e), while the clearly reduced CoV of AR-frequency indicates that the number of ARs over the Atlantic sector is relatively constant compared to other sectors (Figure 9f). Most notably, the CoV of AR-frequency significantly decreases in all sectors towards warmer climates. Meanwhile, the CoV of AR-intensity significantly increases in all sectors.

These results reveal that the decrease in the CoV of ARPMT (section 3.1; indicating more consistent ARPMT) is not caused by a decrease in the CoV of AR-intensity, but by AR-frequency (also shown by reduced AR-days, section 3.2.1). In other words, the number of ARs reaching the Arctic becomes more consistent and relatively less variable. In contrast, the IAV in the intensity of future ARs increases disproportionately to the mean increase. This is crucial as it reveals that while ARs are getting significantly more consistent, there is increased uncertainty around the amount of moisture ARs carry in any given year (partly caused by increased sizes of future ARs). It is therefore of interest to examine the causes of years with anonymously high or low AR-related moisture transport to the Arctic, as discussed hereafter.

3.2.3 Does the jet position (latitude) drive the interannual variability of Arctic ARs?

Here we examine whether the changes in jet stream location are linked to a change in AR activity, depending on the season and sector. Determining the relationship of jet stream latitude and AR activity on an interannual basis may further help to explain whether mean changes in ARs from the PD to a warmer climate are partly caused by jet stream shifts. This is of relevance, as the mean poleward shift of the jet stream in GCMs may be underestimated (Screen et al., 2022), potentially resulting in inaccurate AR-responses to warmer climates (including this study). On the other hand, the potential underestimation of future Arctic sea ice loss (Z. Liu et al., 2021; Notz & Community, 2020; J. C. Stroeve et al., 2012) and the atmosphere response simulated by GCMs (Smith et al., 2022) could imply an equivalent underestimation of the equatorward jet shift (Ma et al., 2021). Hence, studying the effects

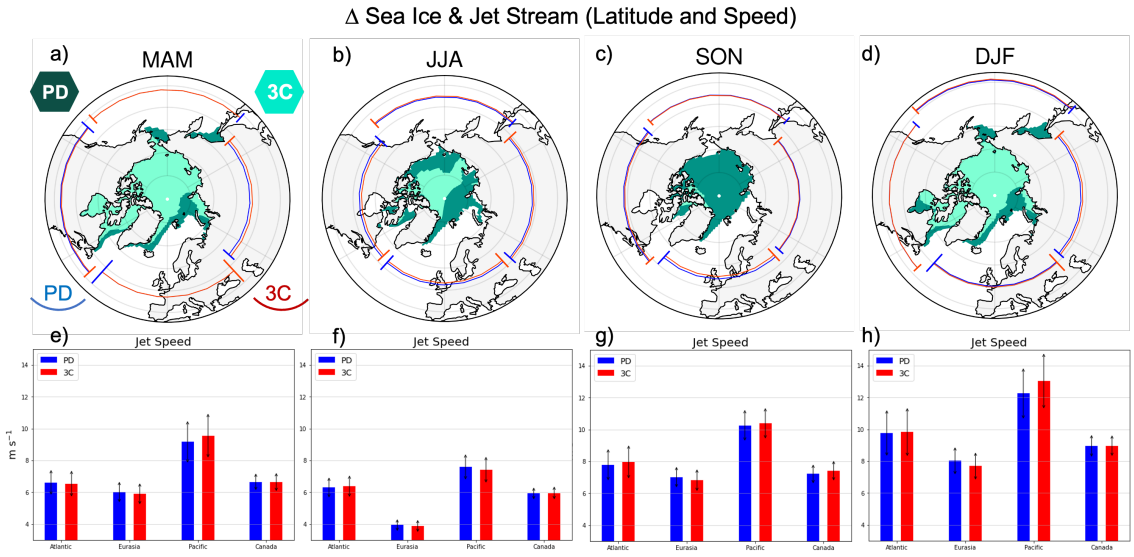

Figure 10: a-d: Seasonal averages of the sea ice extent (SIC >15%) and mean jet latitude in the four sectors, for the present-day (PD) and the +3°C warmer than PI (3C) climate. Vertical blue (red) lines left (right) of the mean jet latitudes represent the respective 95% confidence intervals. e-f: Respective mean jet speed averaged intensity and 95% confidence intervals.

of jet latitude on Arctic ARs on an interannual basis provides information on both ends and offers a reference to different jet and AR scenarios.

To determine changes in the jet stream, we first average the zonal wind at 850 hPA, broadly following Woollings et al. (2010) (we use seasonal values, a fixed pressure level, and various sectors). The mean jet speed in each sector, season and climate is then defined as the maximum westerly wind speed between 30° and 70°. The mean latitude of the jet is quantified by averaging these maximums over the latitudes. We also performed the same analysis using the method applied by Zappa et al. (2018) and Screen et al. (2022), which did not significantly affect results.

Figure 10a-d shows the mean jet latitude for the PD to the 3C climates, as well as the respective mean sea ice extents. In all seasons and most sectors, the shift of the mean jet latitude is minimal. The poleward shift towards warmer climates as found in some GCMs is only apparent in the Atlantic and Canadian sector during summer and autumn (Figure 10b&c). In all other seasons and sectors the shift of the mean jet latitude is minimal, except for an equatorward shift of the winter and spring jet stream latitude over Northern Eurasia. Such spatial differences highlight that the weak jet stream response of the zonally averaged mean is partly a result of regional compensations. Furthermore, the weak mean response to future warming does not entail a lack of response, but may still fit into the picture of a more wavy and varying jet stream (Francis & Vavrus, 2015; Overland, 2021), which does

not require a change in mean latitude. Regarding jet speed (Figure 10e-h), we also find no significant spatially or seasonally consistent trends, although different choices in the sector division and size might yield stronger responses. In spite of weak mean changes, a consistent pattern is found in that all sector-specific poleward (equatorward) shifts are associated with increased (decreased) jet speeds.

Next, we discuss whether the IAV of jet stream characteristics influences Arctic ARs. We find that in all regions a poleward shift of the seasonal jet latitude is typically associated with more (less) ARs east (west) of the respective region (Figure 11a-d). The reason for the

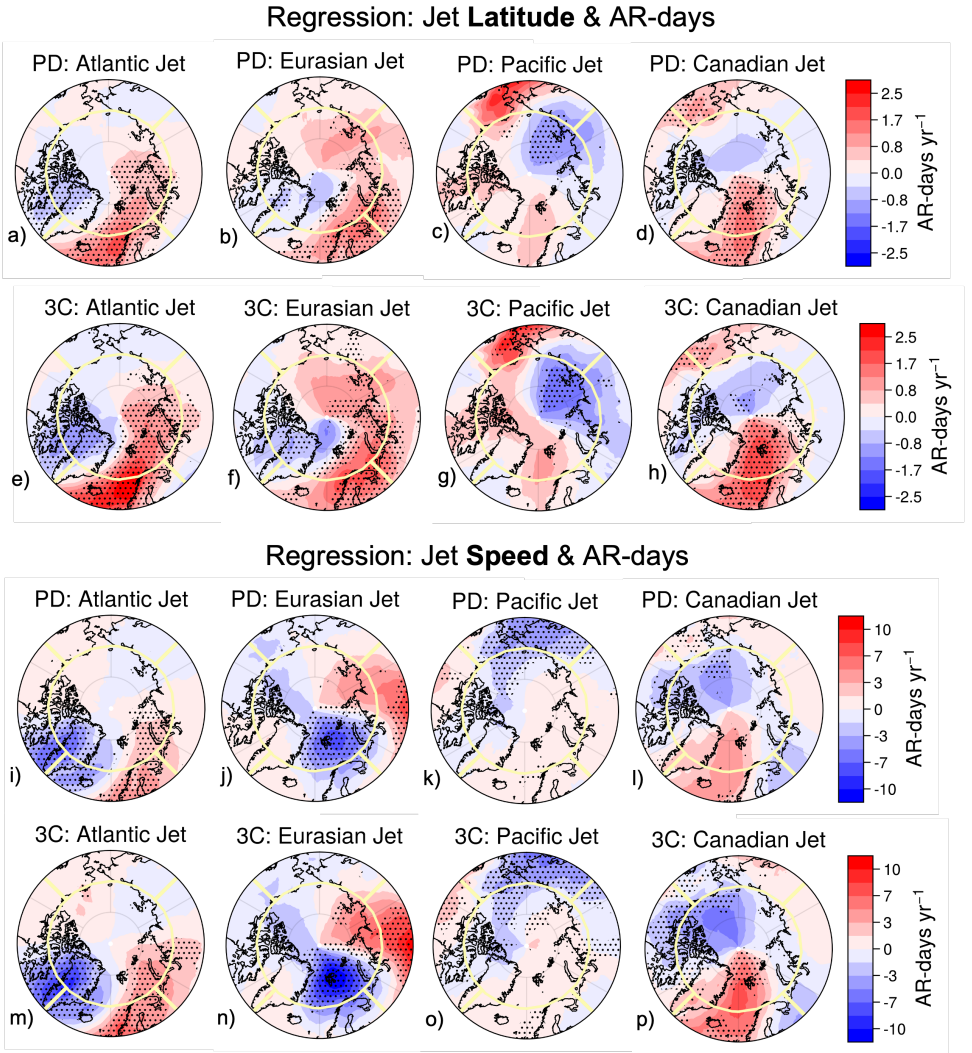

Figure 11: Above: Annual mean of seasonal regressions of the jet latitude in each sector with local AR-days for the PD (a-d) and 3C (e-h) climate. Dotted regions represent areas where the regression is significant (p-value < 0.05) in all seasons. Below: Same as above but for regional jet speeds. Yellow lines represent the 70°N latitude band and sector divisions. Colour scales represent the change in the amount of AR-days per year that a 1° shift in latitude (a-h) or a 1m s^{-1}

change in wind speed (i-p) would induce.

decrease in ARs at the western side of each sector is partly caused by a concurrent increase in jet speed (Figure 11i-l), forcing the poleward oriented moisture further west than usual. Over the Pacific Ocean, anomalously higher jet speeds can reduce the amount of annual ARs over the entire sector by 5 less AR-days, and can instead force these ARs to reach Northern Canada (Figure 11k). The reason for why this pattern is less obvious over the Atlantic Ocean is likely due to the choice of our sector division (the Atlantic sector includes considerably more land regions with reduced wind speeds; Figure 10, e-h). Similarly, years in which the Canadian jet is stronger (and located further north) results in increased AR-days over the Atlantic (Figure 11d,l). Our results further suggest a comparable influence across sectors on ARs reaching the Arctic, implying that the net amount of ARs reaching the Arctic in any given year is influenced and likely compensated by regional differences in jet speed and latitude. These regional differences highlight the importance of examining jet sections rather than global mean jet properties.

In a +3°C warmer climate relative to PI, we find stronger regressions between jet stream latitude (Figure 11 e-h) and Arctic AR-days (Figure 11 m-p). To first degree, these higher regression coefficients are likely a by-product of an Arctic-wide increase in AR-days (Figure 6b). From this we can once more infer that the overall increase in Arctic ARs is not primarily caused by dynamic changes. That said, we find a warming-induced increase in the amount of grid points north of 70°N which are significantly influenced by jet variations, indicating that the Arctic climate under continued warming will be more connected to the dynamics in lower latitudes. In other words, while the main increase in ARs in our 3C simulations is mainly a result of increased moisture (thermodynamic), the dynamic component is still required to transport the moisture to even higher latitudes. The assumption of a weak future poleward shift of the jet latitude in the Atlantic sector during summer and autumn (Figure 10b&c) would thus favour more ARs over the Barents and Kara Sea, and less ARs over Greenland. Such a pattern indeed appears in the dynamic AR-response to increased warming (Figure 6d), suggesting that the local trends in dynamic AR-responses are partly caused by a poleward shift of the Atlantic jet. The regressions showed very similar patterns across seasons (with strongest regressions in summer due to higher AR occurrences).

To summarize, we did not find significant changes in the mean location and speed of the jet stream (in agreement with most GCMs), apart from a slight poleward shift in warmer seasons in the Atlantic and Canadian sectors. It is important to note that these weak/non-existent mean shifts 1) do not imply that the dynamical behaviour jet streams and storm tracks in the models are unaffected by global warming, and 2) are potentially 'underestimated' in current GCMs due to potentially inaccurate sensitivities or parametrizations (e.g. too weak eddy feedback, Screen et al. (2022)). In our EC-Earth simulations, the amount of

ARs that reach the Arctic in any given year and season is strongly linked to the position of the jet stream. For most anomalous poleward locations and increased speed of the jet in any sector, we found a distinct spatial pattern of increased AR-days in the south-eastern part of this sector and the western part of the subsequent sector to the east. Hence, the amount of ARs reaching any Arctic region significantly depends on the jet location and speed southwest of the region. With increased ARs in a warmer climate this relation strengthens, suggested by increased significance in affected regions north of 70°N.

3.3 Effect of ARs on Arctic Climate

3.3.1 Annual Means of Seasonal Anomalies

This section discusses the effect of ARs on Arctic surface air temperature (SAT), precipitation (PR) and sea ice concentration (SIC) on interannual time scales. As a first step, we regressed sector-specific ARPMT (crossing 70°N) with 2D fields of the three variables. In Figure 12 we show annual means of seasonal regressions (i.e. regions where in all seasons the regression slope was significant). We generally see a fairly similar spatial pattern across seasons, with strongest regressions in winter (partly caused by our annual mean threshold which limits winter ARs, increasing the regression strength). Hence we here present annually averaged regressions, and discuss seasonal differences in the following section 3.3.2. We find that the region where ARs cross 70°N distinctly determines the local effect of ARs on PR, SAT and SIC. This finding holds true for the warmer climate (3C), but in most cases (sectors and variables), the regression strength weakens (Figure 12e-h,m-p,u-x). We hypothesize that this is because ARs in 3C dominate total PMT and are based on the PD moisture threshold: some 3C ARs are therefore relatively weak, while 3C anomalies in SAT, PR and SIC are relative to the 3C climate and therefore more 'anomalous'. This results in a reduced average sensitivity of the variables to ARs in 3C.

In terms of surface warming, we find that ARs originating from all sectors increase SAT locally in the respective regions north of the sector. Especially ARs originating from the Eurasian sector have a large impact on local SAT: even a 100 kg m^{-1} s^{-1} increase in Eurasian ARPMT (which is less than half of 1-sigma) can warm up the surface over Northern Eurasia and nearby ocean waters by up to 5°C (Figure 12b; 7°C in winter, not shown). Following observation-based studies, we suggest that the dominating process driving these higher SAT are downwelling longwave fluxes (You et al., 2021; Hegyi & Taylor, 2018). While turbulent sensible heat fluxes could also play a role, the warm air transported by ARs increases the stability of the lower atmosphere, hindering the warm air aloft to reach the colder surface. Komatsu et al. (2018) found observational evidence that warm air masses transported by Siberian ARs ascend when reaching the colder surface air over sea ice. This may explain

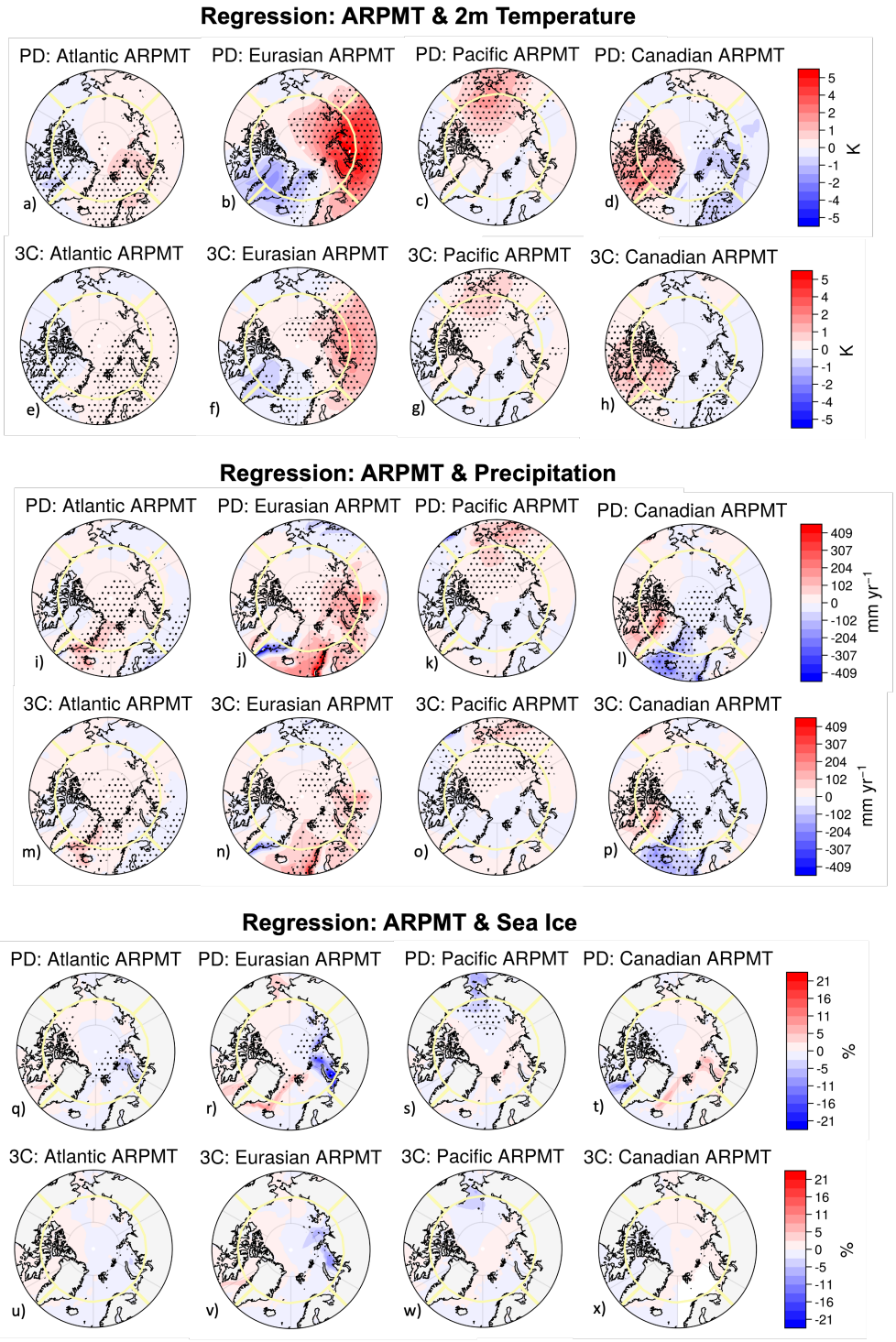

Figure 12: Annual mean of seasonal regressions of ARPMT (here in kg^{-100} m^{-1} s^{-1}) in each sector with local temperature (a-h), precipitation (i-p) and sea ice (q-x) for the PD and 3C climate. Dotted regions represent areas where the regression is significant (p-value < 0.05) in all seasons. Yellow lines represent the 70°N latitude band and sector divisions.

why the effect of ARPMT on SAT is strongest for ARs originating from the Eurasian and Canadian sector (Figure 12b,d), which are dominantly transported to continental regions (i.e. the Northern Eurasian coastline and Greenland) instead of ocean waters. Over the central Arctic Ocean, SAT are moderately and fairly equally affected by the amount of ARPMT originating from the Atlantic, Eurasian and Pacific sectors (up to 2°C per 100 kg m^{-1} s^{-1} on average). Over Greenland, SAT are only significantly raised by ARs from the Canadian (and to a small degree the Atlantic) sector.

The PR response to increased ARPMT via the Atlantic and Pacific sectors is similar to the SAT response: increased moisture transport results in increased PR in the respective Atlantic/Pacific ocean basins and is capable of reaching areas around the North Pole (Figure 12i,k). Interestingly, Arctic ARs entering from continental Eurasia are not only associated with increased PR in the Eurasian Arctic sector, but also decreased (increased) PR over Southeast Greenland (the Northeastern Atlantic). Patterns like these can be caused by changes in large-scale atmospheric modes such as the NAO; for example, Luo et al. (2016) showed that enhanced Ural Blocking drives more moisture from Eurasia into the Arctic, and is also linked to a positive NAO mode (which would induce a North Atlantic PR pattern as in Figure 12j). Increased Canadian ARPMT results in increased PR over the West coast of Greenland and is associated with decreased PR over the East coast. Possible driving mechanisms include an enhanced GBH, which (due to the strengthened anticyclonic circulation) typically decreases PR over Southeast Greenland and the Northern Atlantic. Such interrelations highlight that simple correlations and regressions are not always representing direct impacts. However, we found a robust pattern of increased PR north of the respective sector with high ARPMT, where local PR can increase up to 300 mm yr^{-1} per 100 kg m^{-1} s^{-1} of ARPMT (as in the Eurasian sector; Figure 12j).

The effect on sea ice north of 70°N is relatively subtle, where the total amount of significantly affected regions is smaller compared to SAT and PR. While atmospheric processes can cause strong melt episodes of sea ice, the sea ice condition is also strongly affected by variations in ocean temperature, which can melt sea ice from below. Nonetheless, we find that especially ARs from Eurasia can reduce SIC in the Kara Sea by over 20% (Figure 12r). In addition to increasing local SAT as shown before (Figure 12b), this indicates that a large amount of the transported energy is used to melt sea ice. We also see regions where the sea ice response is significantly positive, but our sector analysis suggests that this might not represent a direct response to increased ARs; these positive sea ice anomalies are only found north and west of 1) Canada and 2) Greenland in years with anomalously high ARPMT from the 1) Atlantic and 2) Eurasian sector, instead of the 1) Canadian, and 2) Atlantic sector, from which the associated ARs would reach these regions. Rather, they could present

another indicator of climate mode states. For example, higher SIC over Northern Canada during high Atlantic ARPMT years (Figure 12q) may be related to the positive phase of the NAO, which is associated with increased North Atlantic ARs (I. Benedict et al., 2019) as well as increased SIC near Canada (Johnston et al., 2005; Qian et al., 2008). However, this does not imply that all ARs in our simulations result in reduced SIC, but that the melt effect tends to dominate the snow-induced effect.

To conclude, increased ARPMT locally increases SAT and PR directly north of the sector-dependent intrusions, and is dominantly linked to reduced sea ice in the respective regions. SATs over the Arctic Ocean increase most in response to high ARPMT reaching from continental regions. The PR response to ARs originating from the Atlantic, Eurasian, and Pacific sector is significant even north of 80°N, whereas Canadian ARs 'only' increase PR near the Canadian archipelago. The sector distinction of ARPMT offered a more robust evidence that the dominating effect on annual SIC is negative (i.e. high ARPMT is linked to reduced SIC). However, season-specific or delayed sea ice responses to ARs (e.g. P. Zhang et al., 2023) are partly hidden in the annual average of seasonal regressions. Therefore, seasonal differences and lags in the response of SAT, PR and SIC are discussed in the following.

3.3.2 Seasonal Extreme Events

Lastly we discuss seasonal differences in the context of extreme ARPMT and Arctic climate events. To do so, we filtered out area-averaged extreme events for ARPMT (across 70°N) and the other variables (north of 70°N). In contrast to section 3.3.1 we investigate the seasonal sum of ARPMT reaching the Arctic from all sectors. For each season and variable, we narrow down the number of events to 100 which all lie above 1.4-sigma. This leaves us with the 100 most extreme events out of 1,600 seasonal means. For consistency, we also used the same 1,600 years to investigate annual means.

As expected, we find that the mean of the 100 extreme anomalies in the 3C climate is higher than the mean of the present-day anomalies in all seasons (Figure 13). However this increase is modest compared to the mean increase (Figure 13a), which is in agreement with the earlier results of a decreased CoV of ARPMT. For example, the mean of ARPMT crossing 70°N in winter increases by 211% from PD to 3C, whereas the mean of extreme winter anomalies only increases by 158%. We also did not find any significant increase or decrease in the number of simultaneous extreme events of ARPMT with most variables in response to a warmer climate, suggesting that the Arctic climate will remain equally affected by extreme AR events in the future.

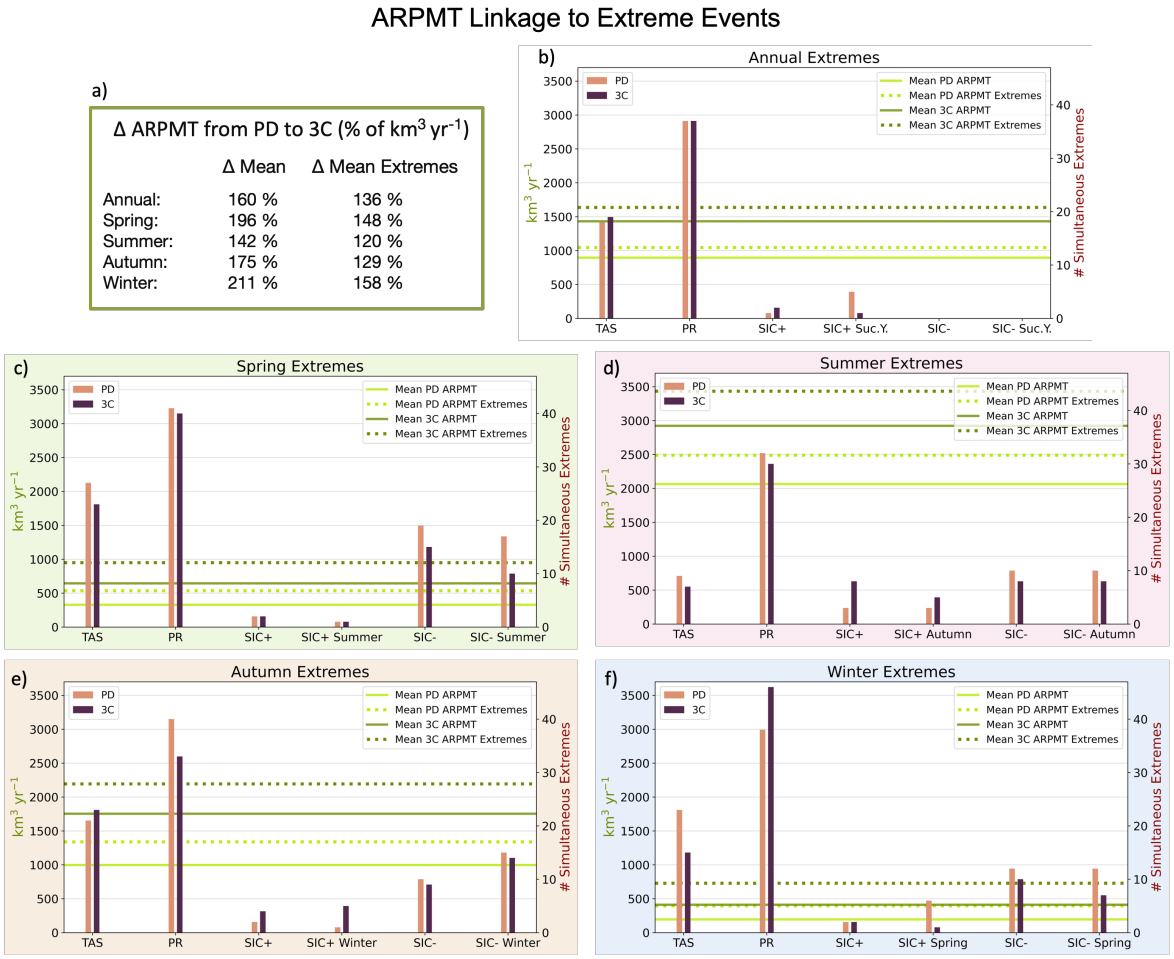

Figure 13: a: Overview of the relative increase of mean ARPMT (left column) and mean of 100 ARPMT extreme events (right column) of each season and climate. b: Light (Dark) green solid horizontal line represents the mean of annually averaged total ARPMT in the PD (3C) climate. Dotted lines represent the respective mean of the 100 most extreme ARPMT events out of 1,600 years. The vertical bars indicate the number of events where in the same year the PR, SAT or sea ice was one of the highest (SIC+) or lowest (SIC-) in the PD (orange) and 3C (brown) climate. For sea ice, also the effect on the sea ice area in the following year (Suc. Y.) or season is shown. c-f: Same as b) but for individual seasons.

Annually averaged, 18 out of the 100 most extreme ARPMT seasonal events coincide with the warmest surface air anomalies. Spring and winter SAT show the greatest response to extreme ARPMT anomalies, with up to 27 years coinciding with extreme ARPMT anomalies. The colder seasons are generally more sensitive to extreme PMT events, which can significantly increase the downward longwave radiation (Woods et al., 2013). In the summer, only 9 of the extreme ARPMT events coincide with any of the 100 warmest Arctic summers.

Consistent with the regressions above, extreme PR shows the strongest link to extreme ARPMT in all seasons. The number of high PR events coinciding with the years of strongest

ARPMT events is fairly persistent across seasons, with 32 (summer) to 41 (spring) simultaneous seasonal events in the present-day climate. As shown earlier, almost all sectors induce a significant PR increase even north of 80°N (Figure 12i-k). With increased warming, the amount of simultaneous PR and ARPMT events slightly decreases in most seasons except winter. In 3C winters, nearly half (46) of all 100 ARPMT events co-occur with the 100 most intense Arctic PR years.

We did not find any cases where any of the 100 lowest annually averaged SIC occurred in one of the highest ARPMT years (Figure 13b). Despite the lack of an annual relation between extreme ARPMT and low SIC events, we found significant decreases of SIC in response to extreme ARPMT events in all seasons (Figure 13c-f). Out of the 100 most extreme ARPMT events, we found at least 10 events where the same as well as the subsequent season showed one of the 100 lowest SIC. The number of cases in which either the same season or the following season showed decreased SIC is very similar, which signifies the sustained melt effect of increased water vapour and temperature over sea ice. The signal is strongest in spring (19 simultaneous events in the PD climate), where the effect on SAT and PR is also largest. In all seasons, the number of simultaneous low SIC and ARPMT extreme events slightly decreases towards 3C. This is likely due to a significantly smaller sea ice area in 3C which is limited to the central Arctic Ocean 10). While we detected a small amount of cases with increased SIC in either the same year or the following year of extreme annual ARPMT events, the number of such events is too small to robustly infer a direct effect (i.e. increased snowfall inducing more ice growth and/or protecting it from melting). However, we found a significant increase in simultaneous extreme high SIC and ARPMT events in summer and autumn from the PD to the 3C climate, with up to 8 simultaneous extreme ARPMT and high SIC summer or autumn seasons. A possible explanation is that the sea ice- covered area in summer and autumn in the 3C climate is located very far north (Figure 10b,c), where temperatures are low enough to allow part of the moisture brought by extreme ARPMT events to fall as snow. However we refer back to the ARPMT and SIC regressions, which revealed that the areas with increased SIC did not lie within the AR pathways and were more likely a characteristic byproduct of climate modes such as the NAO. The strength of e.g. a positive NAO phase and its consequence on SIC could thus play a role on whether the area-averaged sea ice response in our results to increased ARPMT is dominantly positive or negative. Therefore our results strongly suggest a primarily negative direct SIC response to ARPMT in both the present-day and a warmer climate, which is in line with P. Zhang et al. (2023).

In short, extreme ARPMT events are strongly linked to extreme anomalies in Arctic SAT and PR in all seasons. Extremes in PR are most likely to occur simultaneously to ex-

treme ARPMT events, with up to 46% of the most extreme winter ARPMT and PR events occurring in the same year. Extreme anomalies in SAT are also more likely to coincide with extreme ARPMT events in the colder spring and winter seasons, whereas summer temperatures are less sensitive to anomalous ARPMT events, which in part is due to our choice of threshold), but also a sign of increased local processes affecting the Arctic climate, such as variations in surface shortwave heating, surface albedo and local moisture uptake from areas with reduced sea ice (Holland & Landrum, 2015; Vázquez et al., 2017).

3.4 Caveats

This study contains a number of choices that potentially affect the results. We stress that all present-day and future ARs are calculated using an annual-mean threshold. This allowed us to directly compare individual seasons, but implies that the absolute amount of ARs and ARPMT in each season could be considered as over- or underestimated considering the seasonally varying mean conditions. For example, due to lower moisture availability in colder seasons we would capture more winter ARs when using a seasonal threshold, but they would carry significantly less moisture and may have less of an impact compared to summer ARs. Furthermore, our results are limited to the model-dependent representation of the present-day and future climate in EC-Earth2.3, e.g. modes of climate variability or the position and strength of the jet stream (C. Liu & Barnes, 2015; Neff, 2018; I. Benedict et al., 2019; Ma et al., 2021; Gao et al., 2015). For example, the poleward shift in our Atlantic jet and ARs could be underestimated, as the present-day North Atlantic jet in EC-Earth2.3 shows a poleward displacement compared to ERA5 (Döscher et al., 2022; Hazeleger et al., 2012). Lastly, the relation of ARs to Arctic climate as presented in this study is limited to a simple linear regression. Additional investigations of responsible processes could increase certainty about the direct effect of ARs on Arctic climate variations.

4 Conclusions

We evaluated Arctic ARs and moisture transport using long continuous coupled model simulations from EC-Earth2.3 to robustly investigate the influence of AR variability on Arctic climate. AR characteristics are comparable between ERA5 the present-day climate in EC-Earth. The application of a fixed relative as well as a relative method for the detection of future ARs allowed us to identify whether future AR changes are primarily caused by thermodynamic changes or are also dynamically driven.

Firstly, we showed that the increase in total PMT variability is weak compared to the increase in mean PMT. Contrary results of other studies that imply a slight increase

in the CoV of PMT are likely based on a simplified PMT calculation that includes EMT, which show opposite CoV trends to strictly northward PMT. Our results thus allude to a more consistent, less variable PMT to the Arctic, which is mainly caused by the strong increase in moisture transported by ARs. In a +3°C warmer than PI climate, 95% of the additional PMT is carried by ARs, increasing the total share of ARPMT to PMT from 42 to 53%. Correspondingly, the PMT carried by ARs becomes more consistent and less variable from year to year; scaling the IAV of ARPMT by its mean suggests a relative decrease in variability that is significant in all seasons and strongest in winter and spring. By distinguishing AR-intensity from AR-frequency, we showed that this decrease in ARPMT CoV is not caused by a less variable amount of moisture content per AR (intensity), but of AR-days per year (frequency). Simply put, Arctic AR-days are more consistent in warmer climates, but the transported moisture per AR will be highly variable.

The Arctic-wide mean increase in ARs in our 3C simulation is almost exclusively caused by significantly higher atmospheric moisture levels. Dynamical changes are merely of secondary importance in generating future AR changes, but can regionally amplify (as over the North Atlantic) or dampen (as over Greenland and most Arctic Ocean areas) the moisture-induced increase in ARs. However we reiterate that dynamical responses strongly depend on the model-specific dynamic mean state and sensitivity to future warming. For example, the majority of additional ARs in the 3C simulations reach the Arctic from the Atlantic instead of the Pacific sector, which is likely a side effect of a poleward shift of the North Atlantic jet stream (as shown by more future AR-days in r3C).

The amount of ARs reaching any Arctic region in our simulations significantly depends on the jet location and speed southwest of the region. For most anomalous poleward locations and increased speed of the jet in any sector, we found a distinct spatial pattern of increased AR-days in the south-eastern part of this sector and the western part of the subsequent sector to the east. With increased ARs towards a warmer climate, this relation is strengthening, shown by increased significance in affected regions north of 70°N. We did not find strong changes in the mean latitude and speed of the jet stream in most seasons and sectors. However these non-existing mean trends of jet latitude and speed may be incorrectly represented in most current GCMs, which also affects AR changes (Screen et al., 2022; Ma et al., 2021). Assuming a climate change-induced equatorward shift of the North Atlantic jet as suggested by Screen et al. (2022), more (less) ARs would reach Greenland (Northern Europe and the Barents and Kara Seas) (Figure 11). That said, mean changes in jet properties towards warmer climates may not be very noticeable due to strong inter-annual variations which are often linked to climate modes such as the NAO or the GBH (I. Benedict et al., 2019; J. J. Benedict et al., 2019; Barrett et al., 2020; Rimbu et al., 2007).

Our results provide a reference for common jet-AR interactions and suggest that jet stream variability and AR occurrences are most robustly linked on a regional basis.

Increased ARPMT is directly linked to increases in Arctic SAT and PR and decreases in sea ice. We have shown that the particular affected areas are mostly limited to the precise location of ARs (i.e. north of the respective sector of the AR 'entrances'). This holds true for the PD as well as the 3C climate (in which regressions were even lower, probably in response to the increased consistency of ARs). By examining extreme events in addition to annual seasonal-based regressions, we established that the predominant effect of ARs on sea ice is negative in all seasons and both climates. However, the SIC sensitivity to increased ARPMT appears much weaker compared to PR and SAT, due to several possible factors such as strong regional differences (Figure 12), including negative (and thus compensating) signals, or the ability of sea ice to quickly recover from melt episodes. Our results suggest that ARs originating from Eurasia have the largest effect on Arctic climate variability, especially on SAT and SIC. Extreme anomalies in SAT and PR are most likely to coincide with extreme ARPMT events in the colder spring and winter seasons. As for PR, up to 46% of the most extreme winter ARPMT and PR events occur in the same year.

The largely unchanged or even negative strength in the relation between ARPMT and Arctic climate variability towards continuous warming is very likely a sign of the increased consistency of ARs, in addition to the increased importance of local Arctic processes. The relatively low variability and cases of extreme events compared to mean changes in ARs should thus be taken in context of the possible implications in a warmer Arctic climate, in which ARs penetrate further north, and increased mean temperatures cause more PR to fall as rain instead of snow, further accelerating Arctic amplification.

Appendix A

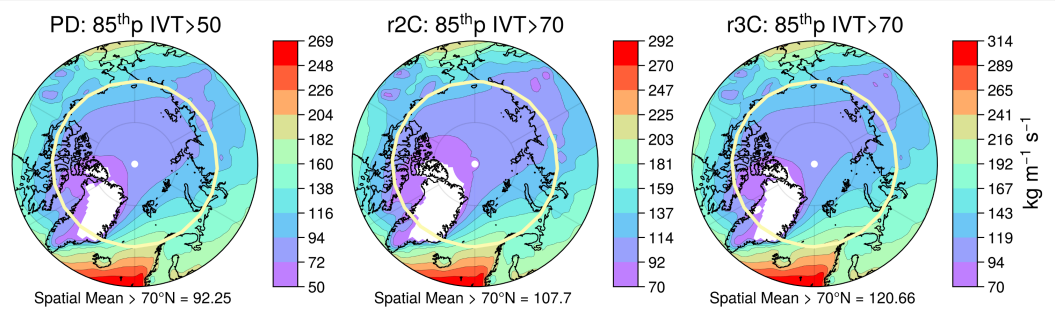

Figure A1: Mean IVT in the EC-Earth present-day, 2C and 3C climates, plotted behind three different masks indicating the effect of the minimum IVT thresholds of 50 kg m^{-1} s^{-1} for the present-day climate and 70 kg m^{-1} s^{-1} for the future climates.

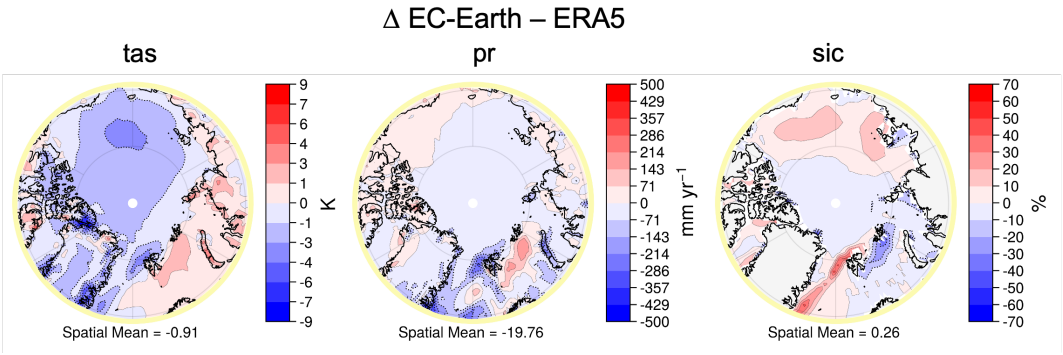

Figure A2: Spatial mean difference of annual surface air temperature (tas), precipitation (pr) and sea ice concentration (sic) north of 70°N between EC-Earth (present-day ensemble) and ERA5 (2005-2020).

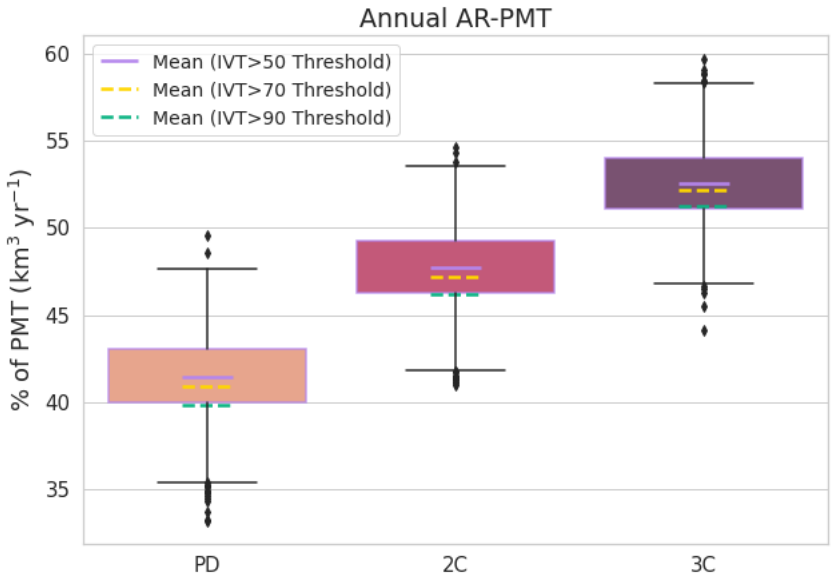

Figure A3: Annually averaged AR-related poleward moisture transport (ARPMT) and quartiles and outliers of the present-day (PD), +2°C warmer than PI (2C) and +3°C warmer than PI (3C) EC-Earth climate runs. The average % of ARPMT is also shown for the 3 different thresholds used.

Acknowledgments

We acknowledge the EC-Earth consortium for their contribution to the development of the EC-Earth climate model. The authors declare that they have no conflicts of interest. All EC-Earth simulation data can be obtained by contacting the authors.

References

Allan, R. P., Liu, C., Zahn, M., Lavers, D. A., Koukouvagias, E., & Bodas-Salcedo, A. (2014). Physically Consistent Responses of the Global Atmospheric Hydrological Cycle in Models and Observations. *Surveys in Geophysics*, *35*(3), 533–552. doi: 10.1007/s10712-012-9213-z

Bachand, C. L., & Walsh, J. E. (2022). Extreme precipitation events in alaska: Historical trends and projected changes. *Atmosphere*, *13*(3), 388.

Bao, J., Michelson, S., Neiman, P., Ralph, F., & Wilczak, J. (2006). Interpretation of enhanced integrated water vapor bands associated with extratropical cyclones: Their formation and connection to tropical moisture. *Monthly weather review*, *134*(4), 1063–1080.

Barnes, E. A., & Screen, J. A. (2015). The impact of arctic warming on the midlat-

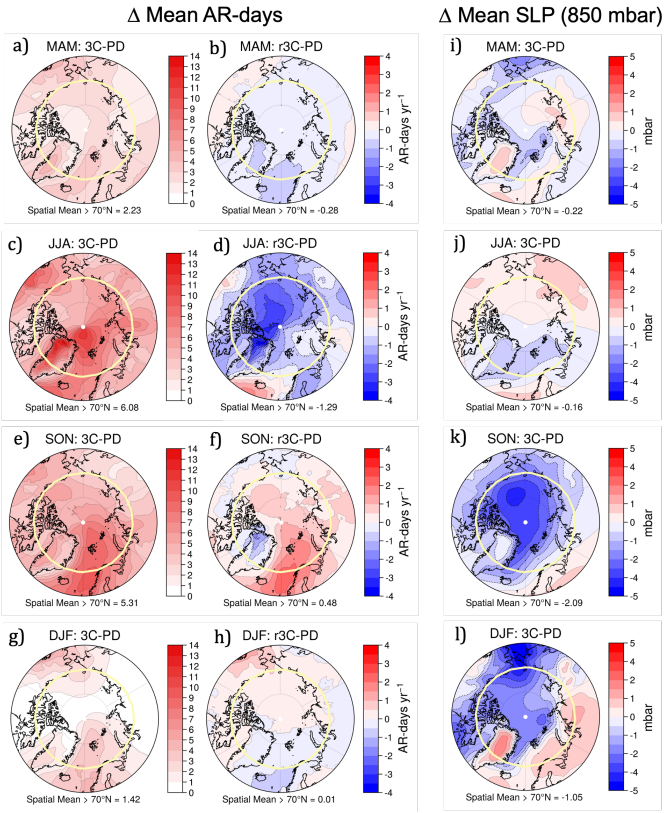

Figure A4: Left panel: Absolute (a,c,e,g) and dynamic-sensitive (b,d,f,h) change of AR-days from the PD towards the 3C climate for each season. Right panel: Changes in sea level pressure at 850 mbar from the PD towards the 3C climate for each season (i,j,k,l).

itude jet-stream: Can it? has it? will it? *Wiley Interdisciplinary Reviews: Climate Change*, *6*(3), 277–286.

Barrett, B. S., Henderson, G. R., McDonnell, E., Henry, M., & Mote, T. (2020). Extreme greenland blocking and high-latitude moisture transport. *Atmospheric Science Letters*, *21*(11), e1002.

Benedict, I., Ødemark, K., Nipen, T., & Moore, R. (2019). Large-scale flow patterns associated with extreme precipitation and atmospheric rivers over Norway. *Monthly Weather Review*, *147*(4), 1415–1428. doi: 10.1175/MWR-D-18-0362.1

Benedict, J. J., Clement, A. C., & Medeiros, B. (2019). Atmospheric blocking and other large-scale precursor patterns of landfalling atmospheric rivers in the north pacific: A cesm2 study. *Journal of Geophysical Research: Atmospheres*, *124*(21), 11330–11353.

Bengtsson, L., Hodges, K. I., Koumoutsaris, S., Zahn, M., & Keenlyside, N. (2011). The changing atmospheric water cycle in Polar Regions in a warmer climate. *Tellus, Series A: Dynamic Meteorology and Oceanography*, *63*(5), 907–920. doi: 10

.1111/j.1600-0870.2011.00534.x

Bintanja, R., & Selten, F. M. (2014). Future increases in Arctic precipitation linked to local evaporation and sea-ice retreat. *Nature*, *509*(7501), 479–482. doi: 10.1038/nature13259

Bintanja, R., van der Wiel, K., van der Linden, E. C., Reusen, J., Bogerd, L., Krikken, F., & Selten, F. M. (2020). Strong future increases in Arctic precipitation variability linked to poleward moisture transport. *Science Advances*, *6*(7), 1–7. doi: 10.1126/sciadv.aax6869

Bogerd, L., van der Linden, E. C., Krikken, F., & Bintanja, R. (2020). Climate State Dependence of Arctic Precipitation Variability. *Journal of Geophysical Research: Atmospheres*, *125*(8). doi: 10.1029/2019JD031772

Chen, G., & Held, I. M. (2007). Phase speed spectra and the recent poleward shift of southern hemisphere surface westerlies. *Geophysical Research Letters*, *34*(21).

Collow, A. M., Shields, C. A., Guan, B., Kim, S., Lora, J., McClenny, E., ... others (2022). An overview of artmip's tier 2 reanalysis intercomparison: Uncertainty in the detection of atmospheric rivers and their associated precipitation. *Journal of Geophysical Research: Atmospheres*, *127*(8), e2021JD036155.

Döscher, R., Acosta, M., Alessandri, A., Anthoni, P., Arsouze, T., Bergman, T., ... others (2022). The ec-earth3 earth system model for the coupled model intercomparison project 6. *Geoscientific Model Development*, *15*(7), 2973–3020.

Espinoza, V., Waliser, D. E., Guan, B., Lavers, D. A., & Ralph, F. M. (2018). Global analysis of climate change projection effects on atmospheric rivers. *Geophysical Research Letters*, *45*(9), 4299–4308.

Francis, J. A., & Vavrus, S. J. (2015). Evidence for a wavier jet stream in response to rapid arctic warming. *Environmental Research Letters*, *10*(1), 014005.

Gao, Y., Lu, J., Leung, L. R., Yang, Q., Hagos, S., & Qian, Y. (2015). Dynamical and thermodynamical modulations on future changes of landfalling atmospheric rivers over western north america. *Geophysical Research Letters*, *42*(17), 7179–7186.

Gimeno, L., Vázquez, M., Nieto, R., & Trigo, R. M. (2015). Atmospheric moisture transport: the bridge between ocean evaporation and arctic ice melting. *Earth System Dynamics*, *6*(2), 583–589.

Gimeno-Sotelo, L., Nieto, R., Vázquez, M., & Gimeno, L. (2019). The role of moisture transport for precipitation in the inter-annual and inter-daily fluctuations of the arctic sea ice extension. *Earth System Dynamics*, *10*(1), 121–133.

Guan, B., & Waliser, D. E. (2015). Detection of atmospheric rivers: Evaluation and

application of an algorithm for global studies. *Journal of Geophysical Research: Atmospheres*, *120*(24), 12514–12535.

Guo, Y., Shinoda, T., Guan, B., Waliser, D. E., & Chang, E. K. (2020). Statistical relationship between atmospheric rivers and extratropical cyclones and anticyclones. *Journal of Climate*, *33*(18), 7817–7834.

Hall, R., Erdélyi, R., Hanna, E., Jones, J. M., & Scaife, A. A. (2015). Drivers of north atlantic polar front jet stream variability. *International Journal of Climatology*, *35*(8), 1697–1720.

Hazeleger, W., Wang, X., Severijns, C., Stefanescu, S., Bintanja, R., Sterl, A., ... van der Wiel, K. (2012). EC-Earth V2.2: Description and validation of a new seamless earth system prediction model. *Climate Dynamics*, *39*(11), 2611–2629. doi: 10.1007/s00382-011-1228-5

Hegyi, B. M., & Taylor, P. C. (2018). The Unprecedented 2016–2017 Arctic Sea Ice Growth Season: The Crucial Role of Atmospheric Rivers and Longwave Fluxes. *Geophysical Research Letters*, *45*(10), 5204–5212. doi: 10.1029/2017GL076717

Hersbach, H., Bell, B., Berrisford, P., Hirahara, S., Horányi, A., Muñoz-Sabater, J., ... Thépaut, J. N. (2020). The ERA5 global reanalysis. *Quarterly Journal of the Royal Meteorological Society*, *146*(730), 1999–2049. doi: 10.1002/qj.3803

Higgins, M. E., & Cassano, J. J. (2009). Impacts of reduced sea ice on winter arctic atmospheric circulation, precipitation, and temperature. *Journal of Geophysical Research: Atmospheres*, *114*(D16).

Holland, M. M., & Landrum, L. (2015). Factors affecting projected arctic surface shortwave heating and albedo change in coupled climate models. *Philosophical Transactions of the Royal Society A: Mathematical, Physical and Engineering Sciences*, *373*(2045), 20140162.

Johnston, D., Friedlaender, A., Torres, L., & Lavigne, D. (2005). Variation in sea ice cover on the east coast of canada from 1969 to 2002: climate variability andimplications for harp and hooded seals. *Climate Research*, *29*(3), 209–222.

Kidston, J., & Gerber, E. (2010). Intermodel variability of the poleward shift of the austral jet stream in the cmip3 integrations linked to biases in 20th century climatology. *Geophysical Research Letters*, *37*(9).

Kim, B.-M., Hong, J.-Y., Jun, S.-Y., Zhang, X., Kwon, H., Kim, S.-J., ... Kim, H.-K. (2017). Major cause of unprecedented arctic warming in january 2016: Critical role of an atlantic windstorm. *Scientific Reports*, *7*(1), 1–9.

Kim, H.-M., & Kim, B.-M. (2017). Relative contributions of atmospheric energy transport and sea ice loss to the recent warm arctic winter. *Journal of Climate*,

30(18), 7441–7450.

Koenigk, T., Brodeau, L., Graversen, R. G., Karlsson, J., Svensson, G., Tjernström, M., ... Wyser, K. (2013). Arctic climate change in 21st century cmip5 simulations with ec-earth. *Climate dynamics*, *40*(11), 2719–2743.

Komatsu, K. K., Alexeev, V. A., Repina, I. A., & Tachibana, Y. (2018). Poleward upgliding siberian atmospheric rivers over sea ice heat up arctic upper air. *Scientific reports*, *8*(1), 1–15.

Light, B., Smith, M. M., Perovich, D. K., Webster, M. A., Holland, M. M., Linhardt, F., ... others (2022). Arctic sea ice albedo: Spectral composition, spatial heterogeneity, and temporal evolution observed during the mosaic drift. *Elem Sci Anth*, *10*(1), 000103.

Liu, C., & Barnes, E. A. (2015). Extreme moisture transport into the arctic linked to rossby wave breaking. *Journal of Geophysical Research: Atmospheres*, *120*(9), 3774–3788.

Liu, Z., Risi, C., Codron, F., He, X., Poulsen, C. J., Wei, Z., ... Bowen, G. J. (2021). Acceleration of western arctic sea ice loss linked to the pacific north american pattern. *Nature communications*, *12*(1), 1–9.

Luo, D., Xiao, Y., Yao, Y., Dai, A., Simmonds, I., & Franzke, C. L. (2016). Impact of ural blocking on winter warm arctic–cold eurasian anomalies. part i: Blocking-induced amplification. *Journal of Climate*, *29*(11), 3925–3947.

Ma, W., & Chen, G. (2022). What controls the interannual variability of the boreal winter atmospheric river activities over the northern hemisphere? *Journal of Climate*, 1–39.

Ma, W., Chen, G., Peings, Y., & Alviz, N. (2021). Atmospheric river response to arctic sea ice loss in the polar amplification model intercomparison project. *Geophysical Research Letters*, *48*(20), e2021GL094883.

Mattingly, K., Mote, T., & Fettweis, X. (2018). Atmospheric river impacts on greenland ice sheet surface mass balance. *Journal of Geophysical Research: Atmospheres*, *123*(16), 8538–8560.

Nash, D., Waliser, D., Guan, B., Ye, H., & Ralph, F. M. (2018). The role of atmospheric rivers in extratropical and polar hydroclimate. *Journal of Geophysical Research: Atmospheres*, *123*(13), 6804–6821.

Neff, W. (2018). Atmospheric rivers melt greenland. *Nature Climate Change*, *8*(10), 857–858.

Nghiem, S., Rigor, I., Clemente-Colón, P., Neumann, G., & Li, P. (2016). Geophysical constraints on the antarctic sea ice cover. *Remote sensing of Environment*,

181, 281–292.

Notz, D., & Community, S. (2020). Arctic sea ice in cmip6. *Geophysical Research Letters*, *47*(10), e2019GL086749.

Overland, J. E. (2021). Rare events in the arctic. *Climatic Change*, *168*, 1–13.

O'Brien, T. A., Wehner, M. F., Payne, A. E., Shields, C. A., Rutz, J. J., Leung, L.-R., ... others (2022). Increases in future AR count and size: Overview of the ARTMIP Tier 2 CMIP5/6 experiment. *Journal of Geophysical Research: Atmospheres*, *127*(6), e2021JD036013.

Papritz, L., & Dunn-Sigouin, E. (2020). What configuration of the atmospheric circulation drives extreme net and total moisture transport into the arctic. *Geophysical Research Letters*, *47*(17), e2020GL089769.

Payne, A. E., Demory, M. E., Leung, L. R., Ramos, A. M., Shields, C. A., Rutz, J. J., ... Ralph, F. M. (2020). Responses and impacts of atmospheric rivers to climate change. *Nature Reviews Earth and Environment*, *1*(3), 143–157. Retrieved from `http://dx.doi.org/10.1038/s43017-020-0030-5` doi: 10.1038/s43017-020-0030-5

Peings, Y., & Magnusdottir, G. (2014). Response of the wintertime northern hemisphere atmospheric circulation to current and projected arctic sea ice decline: A numerical study with cam5. *Journal of Climate*, *27*(1), 244–264.

Pendergrass, A. G., Knutti, R., Lehner, F., Deser, C., & Sanderson, B. M. (2017). Precipitation variability increases in a warmer climate. *Scientific Reports*, *7*(1), 1–9. Retrieved from `http://dx.doi.org/10.1038/s41598-017-17966-y` doi: 10.1038/s41598-017-17966-y

Qian, M., Jones, C., Laprise, R., & Caya, D. (2008). The influences of nao and the hudson bay sea-ice on the climate of eastern canada. *Climate dynamics*, *31*, 169–182.

Rimbu, N., Lohmann, G., & Grosfeld, K. (2007). Northern hemisphere atmospheric blocking in ice core accumulation records from northern greenland. *Geophysical research letters*, *34*(9).

Rivière, G. (2011). A dynamical interpretation of the poleward shift of the jet streams in global warming scenarios. *Journal of the Atmospheric Sciences*, *68*(6), 1253–1272.

Rutz, J. J., James Steenburgh, W., & Martin Ralph, F. (2014). Climatological characteristics of atmospheric rivers and their inland penetration over the western united states. *Monthly Weather Review*, *142*(2), 905–921. doi: 10.1175/MWR-D-13-00168.1

Rutz, J. J., Shields, C. A., Lora, J. M., Payne, A. E., Guan, B., Ullrich, P., ... Viale, M. (2019). The Atmospheric River Tracking Method Intercomparison Project (ARTMIP): Quantifying Uncertainties in Atmospheric River Climatology. *Journal of Geophysical Research: Atmospheres*, *124*(24), 13777–13802. doi: 10.1029/2019JD030936

Screen, J. A., Eade, R., Smith, D. M., Thomson, S., & Yu, H. (2022). Net equatorward shift of the jet streams when the contribution from sea-ice loss is constrained by observed eddy feedback. *Geophysical Research Letters*, *49*(23), e2022GL100523.

Screen, J. A., Simmonds, I., Deser, C., & Tomas, R. (2013). The atmospheric response to three decades of observed arctic sea ice loss. *Journal of climate*, *26*(4), 1230–1248.

Shields, C. A., & Kiehl, J. T. (2016). Atmospheric river landfall-latitude changes in future climate simulations. *Geophysical Research Letters*, *43*(16), 8775–8782.

Shields, C. A., Rutz, J. J., Leung, L. Y., Martin Ralph, F., Wehner, M., Kawzenuk, B., ... Nguyen, P. (2018). Atmospheric River Tracking Method Intercomparison Project (ARTMIP): Project goals and experimental design. *Geoscientific Model Development*, *11*(6), 2455–2474. doi: 10.5194/gmd-11-2455-2018

Skific, N., Francis, J. A., & Cassano, J. J. (2009a). Attribution of projected changes in atmospheric moisture transport in the Arctic: A self-organizing map perspective. *Journal of Climate*, *22*(15), 4135–4153. doi: 10.1175/2009JCLI2645.1

Skific, N., Francis, J. A., & Cassano, J. J. (2009b). Attribution of seasonal and regional changes in arctic moisture convergence. *Journal of Climate*, *22*(19), 5115–5134.

Smith, D. M., Eade, R., Andrews, M., Ayres, H., Clark, A., Chripko, S., ... others (2022). Robust but weak winter atmospheric circulation response to future arctic sea ice loss. *Nature communications*, *13*(1), 1–15.

Sousa, P. M., Ramos, A. M., Raible, C. C., Messmer, M., Tomé, R., Pinto, J. G., & Trigo, R. M. (2020). North atlantic integrated water vapor transport—from 850 to 2100 ce: Impacts on western european rainfall. *Journal of Climate*, *33*(1), 263–279.

Stroeve, J., Nandan, V., Willatt, R., Dadic, R., Rostosky, P., Gallagher, M., ... others (2022). Rain on snow (ros) understudied in sea ice remote sensing: a multi-sensor analysis of ros during mosaic (multidisciplinary drifting observatory for the study of arctic climate). *The Cryosphere*, *16*(10), 4223–4250.

Stroeve, J. C., Serreze, M. C., Holland, M. M., Kay, J. E., Malanik, J., & Barrett, A. P. (2012). The arctic's rapidly shrinking sea ice cover: a research synthesis.

Climatic change, *110*(3), 1005–1027.

Tan, Y., Zwiers, F., Yang, S., Li, C., & Deng, K. (2020). The role of circulation and its changes in present and future atmospheric rivers over western north america. *Journal of Climate*, *33*(4), 1261–1281.

Tandon, N. F., Gerber, E. P., Sobel, A. H., & Polvani, L. M. (2013). Understanding hadley cell expansion versus contraction: Insights from simplified models and implications for recent observations. *Journal of climate*, *26*(12), 4304–4321.

van der Wiel, K., & Bintanja, R. (2021). Contribution of climatic changes in mean and variability to monthly temperature and precipitation extremes. *Communications Earth {\&} Environment*, *2*(1), 1–11. Retrieved from `http://dx.doi.org/10.1038/s43247-020-00077-4` doi: 10.1038/s43247-020-00077-4

van der Wiel, K., Wanders, N., Selten, F. M., & Bierkens, M. F. P. (2019). Added Value of Large Ensemble Simulations for Assessing Extreme River Discharge in a 2 °C Warmer World. *Geophysical Research Letters*, *46*(4), 2093–2102. doi: 10.1029/2019GL081967

Vázquez, M., Algarra, I., Eiras-Barca, J., Ramos, A. M., Nieto, R., & Gimeno, L. (2018). Atmospheric rivers over the Arctic: Lagrangian characterisation of their moisture sources. *Water (Switzerland)*, *11*(1), 1–14. doi: 10.3390/w11010041

Vázquez, M., Nieto, R., Drumond, A., & Gimeno, L. (2017). Extreme sea ice loss over the arctic: an analysis based on anomalous moisture transport. *Atmosphere*, *8*(2), 32.

Wang, Z., Walsh, J., Szymborski, S., & Peng, M. (2020). Rapid arctic sea ice loss on the synoptic time scale and related atmospheric circulation anomalies. *Journal of Climate*, *33*(5), 1597–1617.

Warner, M. D., & Mass, C. F. (2017). Changes in the climatology, structure, and seasonality of northeast pacific atmospheric rivers in cmip5 climate simulations. *Journal of Hydrometeorology*, *18*(8), 2131–2141.

Warner, M. D., Mass, C. F., & Salathé, E. P. (2015). Changes in winter atmospheric rivers along the north american west coast in cmip5 climate models. *Journal of Hydrometeorology*, *16*(1), 118–128.

Webster, M. A., Parker, C., Boisvert, L., & Kwok, R. (2019). The role of cyclone activity in snow accumulation on arctic sea ice. *Nature communications*, *10*(1), 1–12.

Woods, C., Caballero, R., & Svensson, G. (2013). Large-scale circulation associated with moisture intrusions into the arctic during winter. *Geophysical Research Letters*, *40*(17), 4717–4721.

Woollings, T., Hannachi, A., & Hoskins, B. (2010). Variability of the north atlantic eddy-driven jet stream. *Quarterly Journal of the Royal Meteorological Society*, *136*(649), 856–868.

Wu, Y., Ting, M., Seager, R., Huang, H.-P., & Cane, M. A. (2011). Changes in storm tracks and energy transports in a warmer climate simulated by the gfdl cm2. 1 model. *Climate dynamics*, *37*(1), 53–72.

Yim, B. Y., Min, H. S., & Kug, J.-S. (2016). Inter-model diversity in jet stream changes and its relation to arctic climate in cmip5. *Climate Dynamics*, *47*(1), 235–248.

You, C., Tjernström, M., & Devasthale, A. (2021). Warm-air advection over melting sea-ice: A lagrangian case study. *Boundary-Layer Meteorology*, *179*, 99–116.

Zappa, G., Pithan, F., & Shepherd, T. G. (2018). Multimodel evidence for an atmospheric circulation response to arctic sea ice loss in the cmip5 future projections. *Geophysical Research Letters*, *45*(2), 1011–1019.

Zhang, P., Chen, G., Ma, W., Ming, Y., & Wu, Z. (2021). Robust atmospheric river response to global warming in idealized and comprehensive climate models. *Journal of Climate*, *34*(18), 7717–7734.

Zhang, P., Chen, G., Ting, M., Ruby Leung, L., Guan, B., & Li, L. (2023). More frequent atmospheric rivers slow the seasonal recovery of arctic sea ice. *Nature Climate Change*, 1–8.

Zhang, X., He, J., Zhang, J., Polyakov, I., Gerdes, R., Inoue, J., & Wu, P. (2013). Enhanced poleward moisture transport and amplified northern high-latitude wetting trend. *Nature Climate Change*, *3*(1), 47–51.

Zhang, Z., Ralph, F. M., & Zheng, M. (2019). The relationship between extratropical cyclone strength and atmospheric river intensity and position. *Geophysical Research Letters*, *46*(3), 1814–1823.

Zhu, Y., & Newell, R. E. (1998). A proposed algorithm for moisture fluxes from atmospheric rivers. *Monthly weather review*, *126*(3), 725–735.